

NWP SAF

Satellite Application Facility for Numerical Weather Prediction

Document NWPSAF-MF-VS-004

Version 1.0

31 December 2004

Use of AIRS cloudy radiances

M. Dahoui
Moroccan Meteorological Service

F. Rabier, L. Lavanant
Météo-France

N. Fourrié
CNRS



NWP SAF

Satellite Application Facility for Numerical Weather Prediction

Report of Visiting Scientist Mission

Use of AIRS cloudy radiances

M. Dahoui
Moroccan Meteorological Service

and

F. Rabier*, **L. Lavanant*** and **N. Fourrié****

* Météo-France

** CNRS

NWPSAF-MF-VS-004 Version 1.0

This documentation was developed within the context of the EUMETSAT Satellite Application Facility on Numerical Weather Prediction (NWP SAF), under the cooperation Agreement dated 25 November 1998, between EUMETSAT and the Met Office, UK, by one or more partners within the NWP SAF. The partners in the NWP SAF are the Met Office, ECMWF, KNMI and Météo France.

Copyright 2004, All Rights reserved.

Change record			
Version	Date	Author/changed by	Remarks
1.0	31.12.04	M. Dahoui	

Use of AIRS cloudy radiances

December 31, 2004

M. Dahoui, F. Rabier, L. Lavanant and N. Fourrié

1 Introduction

Use of data from polar orbiting satellites has advanced substantially during the last decade. From the first crude use of retrieved temperature and humidity profiles, raw radiances are now assimilated in various Numerical Weather Prediction (NWP) centres and the impact on forecasts is positive and consistent. Data from the advanced Atmospheric Infrared Sounder AIRS (Aumann et al. 2003, airs.jpl.nasa.gov) are currently widely used in operational or experimental NWP systems. Work is on-going to prepare the use of data from IASI (Phulpin et al, 2002, smc.cnes.fr/IASI/) scheduled to be launched in 2006. Currently, data assimilation systems account only for clear pixels or channels peaking well above the clouds in cloudy pixels. However, dynamically active areas are known to be mainly cloudy (Fourrié and Rabier, 2004, McNally, 2002). Clouds modulate significantly the infrared radiances and make the observation operator highly nonlinear ; weighting functions depend strongly on cloud top pressure (CTP) and cloud amount (CC). Moreover, the NWP systems have not reached enough accuracy to predict clouds close to reality. In addition, cloud modeling inside radiative transfer models is quite simple and needs sophisticated treatment of cloud optical properties. Therefore without a proper treatment of clouds, cloudy data could have a detrimental impact on the analysis and the subsequent forecasts. Use of cloudy radiances is under investigation in several NWP centres. Preliminary one-dimensional studies (Chevalier et al., 2004) demonstrate the capability of variational systems to assimilate selected cloud-affected channels using enhanced cloud schemes. In Météo-France, the clear and cloudy AIRS radiances are routinely monitored. Different cloud detection and characterization schemes (Dahoui et al, 2004) are implemented inside the ARPEGE screening module. The aim of this SAF NWP visiting scientist mission is to go a step ahead towards the assimilation of AIRS cloudy radiances. Two approaches will be used to assimilate useful AIRS cloudy channels directly in the 4D-Var (four dimensional variational) system. Results might provide a strategy for the future use of cloudy radiances.

The first approach makes use of a diagnostic cloud scheme which will be a component of the observation operator. To prepare such assimilation approach it is necessary to perform an extensive evaluation of the diagnostic cloud-scheme. This will help us firstly to appreciate the accuracy of the diagnostic cloud-scheme and secondly to derive observation error statistics (bias, standard deviation) which will be used in the assimilation experiments. We will also evaluate the nonlinearity of the observation operator for each AIRS channel according to the cloud types present in the Field Of View (FOV). The methodology used is similar to Chevalier et al, 2004. In parallel, we will investigate another approach relying

more heavily on the data themselves. Cloud parameters (cloud top pressure and cloud cover) provided by the CO2-slicing algorithm will be used as input to the RTTOV model inside the analysis. A first step would be to use these cloud fields coming directly from the CO2 slicing algorithm and keep them constant throughout the minimisation. In a second step, CO2-slicing cloud fields will be adjusted by a prior 1D-Var. Retrieved cloud fields would then be used as input to 4D-Var.

The plan of the report is as follows. Section 2 presents the variational formalism in four and one dimension. Section 3 outlines the observation operators to be used in the assimilation experiments. It presents validation results. Assimilation experiments of AIRS cloudy radiances are presented in section 4. Conclusions are summarized in section 5.

2 Variational data assimilation theory

2.1 4D-Var assimilation system

Since June 2000, the operational analysis system at Météo-France is a 4D-Var variational analysis system which is similar to the ECMWF 4D-Var (Rabier, 2000). The goal of 4D-Var is to provide the initial state of a forecast model using all the available informations on the atmospheric state. It seeks an optimal balance between the observations and the model by finding a model trajectory $x(t)$ which is as close as possible to the observations available during a time period $[t_0, t_n]$. The model trajectory $x(t)$ is defined by the initial state x_0 at time t_0 . The analysis state is produced through the minimisation of an objective function given by :

$$J(x) = \frac{1}{2}(x_0 - x_0^b)^T B^{-1}(x_0 - x_0^b) + \frac{1}{2} \sum_{i=0}^{i=n} (H_i[x(t_i)] - y_i)^T O_i^{-1} (H_i[x(t_i)] - y_i) + J_c \quad (1)$$

where at time t_i , y_i is a the vector of all observations, O_i is the observation error covariance matrix (measurement errors and representativeness errors), B is the background error covariance matrix and H_i is the observation operator which computes the model equivalent $H_i[x(t_i)]$ of the observation. It contains a model integration from the validity time of x to the time t_i of the observation. The J_c is a dynamical constraint term used to increase the balance in the analysis increment. Superscripts -1 and T denote respectively inverse and transpose matrix. The state obtained by the minimisation of the objective function is a maximum likelihood solution to the problem. The solution is only optimal if the model and observation errors are unbiased and correctly specified. The minimisation of the objective function uses a limited memory quasi newton optimisation program (M1QN3) which requires the computation of the gradient J at each iteration (Gilbert and Lemaréchal, 1989) :

$$\nabla J(x) = B^{-1}(x_0 - x_0^b) + \sum_{i=0}^{i=n} \mathbf{H}_i^T O_i^{-1} (H[x(t_i)] - y_i) \quad (2)$$

For the purpose of assimilation of cloud affected radiances, the observation operator must contain all necessary components to produce and treat cloud fields in order to generate the model equivalent of cloudy radiances. In the framework of this study, two approaches are used to represent the observation operator. The first approach is described in detail in Janisková et al, 2002. It makes use of a diagnostic cloud scheme to produce cloud fields (cloud cover, cloud liquid water and cloud ice water) from the control variables

T , q and p_s . Output cloud fields are supplied as input to the enhanced radiative transfer model RTTOVCLD (Saunders et al, 2002). In the second approach, cloud top pressure and cloud cover are estimated from a prior application of the CO2-slicing (Menzel et al, 1983, Lavanant, 2002) algorithm. Then they are supplied, as input, to the radiative transfer model RTTOV. For the sake of simplicity, cloud parameters will be kept constant during the minimisation process. These two approaches are explained in details in section 4.

2.2 1D-Var assimilation scheme

The principle of 1D-Var is similar to that of 4D-Var, except the fact that the control variable represents a single column and the time dimension is not included. The 1D-Var scheme is used, in this work, to adjust cloud parameters produced by the CO2-slicing method.

Cloud top pressure and cloud cover are added to the control variable x . Initial background values of cloud fields come directly from the CO2-slicing algorithm. The radiative transfer model RTTOV makes use of cloud fields to simulate cloudy radiances by assuming that we have a single cloud layer. The cloud top pressure and cloud cover background errors are fixed respectively to 100 hpa and 0.2. These values are estimated by comparing CO2-slicing cloud fields to a MODIS cloud mask (see Dahoui et al, 2004). This implementation of 1D-VAR is not optimal since background cloud fields are correlated with the observations via the CO2-slicing algorithm.

3 Simulated AIRS cloudy radiances

A key element in the success of the variational data assimilation, is the accuracy and the linearity of the observation operator. It indicates the extent of our capability to represent the observed phenomenon. If the simulated values are very far from the observed ones, no useful information can be extracted and the observation errors are, certainly, biased and therefore, the subsequent analysis is not optimal. It is especially difficult to account for clouds in the observation operator since cloud processes are not well resolved by NWP and radiative transfer models. The on/off nature of clouds and the various threshold switches, inside the cloud schemes, result in significant nonlinearities. Chevalier et al, 2004 shows that it is possible to select cloud-affected channels for which the accuracy and the linearity of the observation operator are enough to be assimilated by the 4D-Var in near-optimal conditions. In this section, the same methodology is used for the evaluation of the accuracy and linearity of the two observation operators used by the two assimilation approaches. The accuracy and linearity are assessed according to cloud height. Cloud characterization is carried out using the CO2-slicing algorithm.

3.1 Bias correction scheme

Before the use of AIRS radiances, the data must be bias-corrected to remove systematic errors intrinsic to the observation operator or to the raw data themselves (Eyre et al. 1992). The scheme used in this study is the so-called Neural Network bias correction scheme (Auligne, T., 2004). The methodology is similar to Harris and Kelly, 2001, but with a non-linear regression. The neural network weights, associated to predictors,

are derived from a learning process performed on dataset declared "active" in former screenings.

3.2 CO2-slicing cloud characterization algorithm

The CO2-slicing method has been extensively used to retrieve cloud top pressure and cloud effective emissivity. The algorithm, based on radiative transfer principles, uses the measured radiances of a subset of AIRS channels selected in the CO2 absorption band, which is very sensitive to the presence of clouds. For each FOV, and for each channel of the subset, the following expression is calculated :

$$F_{k,p} = \frac{(R_{clear}^k - R_{meas}^k)}{(R_{clear}^{k_{ref}} - R_{meas}^{k_{ref}})} - \frac{(R_{clear}^k - R_{cld}^{k,p})}{(R_{clear}^{k_{ref}} - R_{cld}^{k_{ref},p})} \quad (3)$$

where :

- k : channel in the CO2 band
- k_{ref} : reference window channel = 917.27 cm^{-1}
- p : pressure level number
- R_{meas}^k : measured radiance in channel k
- $R_{cld}^{k,p}$: simulated black-body radiance for channel k and at the cloud level p
- R_{clear}^k : simulated clear radiance in channel k

The function $F_{k,p}$ is evaluated for a selected range of pressure levels. The cloud-top pressure $p_{c,k}$ assigned to channel k is the level which minimizes the function.

The final cloud-top pressure p_c assigned to the FOV is obtained by :

$$p_c = \frac{\sum p_{c,k} w_k^2}{\sum w_k^2} \quad (4)$$

with $w_k = \delta F_{k,p} / \delta \ln p$ the derivative of the cloud pressure function.

The effective emissivity is then computed for the reference window channel by :

$$N_\epsilon = \frac{(R_{clear}^{k_{ref}} - R_{meas}^{k_{ref}})}{(R_{clear}^{k_{ref}} - R_{cld}^{k_{ref}})} \quad (5)$$

The method assumes that the cloud is a thin layer. A first test flags the situation as clear if the departure between clear and cloudy radiances is less than the radiometric $noise * \sqrt{2}$ for all channels. In general, the cloud resulting information is flagged bad, if the retrieved cloud emissivity is smaller than 0 or larger than 1.2. 63 AIRS channel were used in addition to the reference AIRS channel 787 (917.27 cm^{-1}).

As in Dahoui et al, 2004, the CO2-slicing technique is used for both cloud detection and cloud characterisation. A rough cloud detection test, based on a threshold on AIRS channel 787, is added inside the algorithm to reinforce the cloud detection decisions.

The CO2-slicing algorithm plays a key role in our present strategy to assimilate cloudy radiances. It is applied, inside the screening module, to perform cloud detection and

to assign, to each AIRS FOV a cloud top pressure and a cloud amount. These cloud parameters are used to make some decisions on the use of AIRS cloudy radiances and they will be supplied, as input, to RTTOV inside the 4D-VAR minimisation. Extensive validation of this technique is done in Dahoui et al. 2004, using a cloud mask derived from MODIS (Platnick et 2003, modis.gsfc.nasa.gov). The CO2-slicing cloud detection and characterisation results are in good agreement with the MODIS cloud mask for clouds above 900 hpa. The sensitivity to clouds is poor near the surface and for fractional clouds.

3.3 Diagnostic cloud scheme

As explained above, the assimilation of cloudy radiances requires sophisticated cloud and radiation schemes to be able to compare observed and simulated radiances. For the radiation scheme, we rely on the RTTOVCLD code. Cloudiness has three origins: large scale over-saturation (stratiform), subgrid shallow convection over-saturation and subgrid deep convection over-saturation. In our context, cloudiness is controlled by a simple diagnostic cloud scheme, developed for the use in the cloud-affected radiance assimilation. It reproduces the main features of the ARPEGE operational cloud scheme (Gérard, L., 2001) but only the large scale cloud processes are taken into account. This limitation is firstly due to some technical reasons, not having to store physical tendencies necessary for the treatment of the convection processes. The second important reason is the fact that large scale processes have a more continuous shape and contain less on/off processes than convective processes. However, it is necessary to limit the assimilation approach, using this simple diagnostic cloud scheme, to only situations dominated by large scale cloudiness.

The developed scheme diagnoses the cloud cover, the cloud liquid water vapour content and the cloud ice water vapour content at 41 vertical levels (corresponding to those of the ARPEGE model) from the temperature and humidity profiles and the surface pressure. The condensed water content is linked, at each level l , to the potential water vapour excess by the following equation :

$$q_{cs}^l = q_{cx} \left[1 - e^{\frac{-\alpha_s(q_v^l - r_c^l q_{sat}^l)}{q_{cx}}} \right] \quad (6)$$

with:

- q_v^l the specific humidity at level l ,
- q_{sat}^l specific humidity of saturation at level l ,
- q_{cx} the maximum sustainable water content,
- r_c^l the critical minimum relative humidity producing a cloud. It is a constant profile computed according to the following relation :

$$r_c^l = 1 - \max(2\sigma^l(1 - \sigma^l)(1 + \sqrt{1.8}(\sigma^l - 0.5)), 10^{-12}) \quad (7)$$

where σ is the vertical coordinate of the pressure divided by the surface pressure.

- α_s a tunable coefficient controlling the amount of condensates, where a cloud already exists with respect to r_c^l .

The cloud cover is evaluated from the condensed water content according to Xu and Randall (1996) formula :

$$PCC^l = \left(\frac{q_v^l}{q_{sat}^l} \right)^{qx} \left[1 - \exp \left(\frac{-\alpha_r q_{cs}^l}{\left[\left(1 - \frac{q_v^l}{q_{sat}^l} \right) q_{sat}^l \right]^\gamma} \right) \right] \quad (8)$$

where qx , α_r and γ are tunable coefficients.

Cloud liquid and solid water vapour contents are computed using the following equations :

$$PQLI^l = q_{cs}^l (1 - f^l(T^l)) \quad PQICE^l = q_{cs}^l f^l(T^l)$$

If $T^l > T_t$ we have $f^l(T^l) = 0$, otherwise :

$$f^l(T^l) = 1 - \exp^{\frac{-1}{2} \left(\frac{T^l - T_t}{T_0} \right)^2} \quad (9)$$

where T_t is the water triple point temperature. Coefficient $T_0 = 11.82$ copes for liquid and solid phase coexistence in the neighbourhood of the triple points.

For a subsequent use in the 4D-Var assimilation system, a linear tangent and adjoint of this scheme are also coded.

The discrimination between convective and large scale cloudiness is performed, inside the screening module, by a simple algorithm. It compares the cloud cover produced by the operational and large scale diagnostic cloud schemes. The comparison is done on the 22 lowest model levels, where convective clouds are generally localized.

For each level j , the algorithm evaluates $\frac{CC_F(j) - CC_{LS}(j)}{CC_F(j)}$, where CC_F denotes the full (large scale + convective) diagnosed cloud cover and CC_{LS} the large scale diagnosed cloud cover. If the averaged value, on the 22 levels, is less than 0.2 the situation is considered as dominated by large scale cloudiness. Otherwise, convective clouds are present on the FOV and consequently the pixel is rejected. The top apnel in Figure 1 shows a typical example of cloud fraction profiles generated by the large scale and the full diagnostic cloud schemes. The large difference between the two profiles indicates that, for this pixel, the large scale cloud scheme is not able to reproduce correctly all features of the full scheme, due to active convection processes. To be more robust, this comparison algorithm could be extended to involve cloud liquid water and cloud ice water.

3.4 Accuracy of the observation operators

As stated above, two observation operators are under evaluation in this study. For each operator, we perform statistics on simulated minus observed AIRS cloudy spectrum, over 4 days in March and 4 days in July 2004. These two time periods are chosen, arbitrarily, to have access to different cloud regimes. Statistics are computed in terms of mean, standard deviation and correlation. Only data over sea are taken into account.

3.4.1 Observation operator with the diagnostic cloud scheme

As a first step we start this evaluation study by a visual comparison between geostationary imagery and the model equivalent using the ARPEGE operational diagnostic cloud scheme (including both stratiform and convective clouds). It is useful because this

operational diagnostic cloud scheme is used to differentiate between FOVs dominated by large scale clouds and those with convection activity. Its large scale part is exactly the same as in the observation operator. Visual comparison (see examples in Figures 2 and 3) indicates that all cloud patterns are well reproduced by the operational cloud scheme over sea and over land. Some differences occur over the tropical area but even there, the cloud scheme seems reliable. A quantitative evaluation of the ARPEGE operational diagnostic cloud scheme is performed by comparing, for different latitude bands, the simulated and observed AIRS cloudy spectrum. Simulated AIRS channels are produced using atmospheric fields from a 6 hour forecast. Figure 4 shows the bias and the standard deviation of the difference between simulated and observed cloudy brightness temperatures (TBs) for a set of 324 AIRS channels. Stratospheric channels, less affected by clouds, are well simulated by the observation operator. The highest values of the standard deviation and bias are observed in the spectral region between 750 cm^{-1} to 1500 cm^{-1} , which is the most affected by clouds. The bias is mainly positive indicating that the model underestimates clouds especially in the tropics.

The same statistics are performed using the large scale diagnostic cloud scheme (see Figure 5). In the mid-latitudes, results are similar to those of the ARPEGE operational cloud scheme. In the tropics, the large scale cloud scheme underestimates the cloud forcing since the convective activity is not taken into account.

Another efficient way to evaluate the observation operator is to calculate the correlation between simulated and observed AIRS cloudy TBs. High correlation values indicate that the diagnostic cloud scheme is able to predict the event of cloud patterns. Figure 6 shows the correlation, by latitude bands, between modelled and observed cloudy spectra. The best values are in the northern high latitudes. Tropics, obviously, have the lowest correlation values since convective systems are not modelled.

3.4.2 Observation operator with the CO2-slicing algorithm

The CO2-slicing method, extensively tested in Dahoui et al., 2004, provides cloud top pressure and cloud cover with a good quality. When compared to MODIS, the CO2-slicing CTP and CC standard deviation errors are, respectively, 100 hpa and 0.2. Use of the CO2-slicing cloud parameters in RTTOV may reduce significantly the departure between simulated and observed cloudy spectrum. Figure 7 presents bias and standard deviation of the difference between simulated and observed AIRS cloudy TBs, with and without the inclusion of the CO2-slicing derived cloud parameters. The same statistics are presented in the case of clear AIRS TBs, for reference. As expected, statistics for stratospheric and upper tropospheric channels are similar in clear and cloudy conditions. For AIRS channels peaking lower in the atmosphere, the use of cloud parameters reduces significantly the difference between observation and model equivalent AIRS cloudy TBs. Standard deviation values of those channels, remain twice as large as those in clear conditions. Assimilation of such channels requires the revision of the observation errors statistics to account for errors introduced by the CO2-slicing scheme.

The use of a prior 1D-VAR to adjust cloud parameters, from the CO2-slicing scheme, may create more balance between simulated and observed TBs. Figure 8 shows the same statistics as in Figure 7 but using 1D-VAR adjusted CO2-slicing CTP and CC. Statistics are very similar in clear and cloudy conditions, except for high wavenumbers, which may appear very interesting for the data assimilation of cloudy radiances. However, the post-processing by the CO2-slicing and 1D-VAR schemes may complicate the shape of errors and create significant correlation between AIRS channels which must be taken into

account, properly, in the assimilation system.

3.5 Linearity of the observation operator

To be optimal, the variational data assimilation requires, for each observation type, to have an observation operator linear, at least in the vicinity of the background. Cloud processes and threshold switches, in cloud schemes, result in nonlinearities in the observation operator. In this study we follow the same methodology as in Chevalier et al, 2004 and Dahoui et al, 2004, to select the AIRS channels for which the observation operator is linear. The linearity is evaluated according to high, medium and low clouds (the cloud classification is from the CO2-slicing technique).

For each AIRS channel and for each cloud type, the correlation between linear and non-linear brightness temperature perturbations is computed. Perturbations taken here are simply the difference between the analysis x_{an} and the background x_b . Analysis profiles are produced by the current ARPEGE operational assimilation cycle. Background profiles are produced by forecasts just prior to the last operational assimilation cycle. For each cloud type, the correlation between the tangent-linear perturbations $\mathbf{H}(x_{an} - x_g)$ and the non-linear ones $H(x_{an}) - H(x_g)$ (where $\mathbf{H}(x_{an} - x_g)$ is the tangent-linear of the observation operator in the vicinity of x_{an} and H the non-linear observation operator) is computed using the ensemble of profiles corresponding to the selected FOVs. As in Chevalier et al, 2004, the linearity assumption is considered as valid only for channels having correlation value more than 0.85. Figure 9 presents, according to cloud height, all AIRS channels having correlation values more than 0.85. For all cloud types, channels around 670 cm^{-1} , 1500 cm^{-1} and 2300 cm^{-1} have a good linear behaviour. In the presence of low clouds, a considerable number of channels, in the most cloud sensitive spectral region from 750 cm^{-1} to 1350 cm^{-1} , show an acceptable linear behaviour.

4 4D-VAR assimilation of AIRS cloudy radiances

The use of satellite cloudy radiances is one of the most active research fields in atmospheric data assimilation. An important work was carried out at several NWP centres, to study the various aspects of the problem. The main goal of nearly all studies is how to conceive accurate observation operators, for cloud assimilation purposes, with a minimum of inherent nonlinearities. Observation operators must, in addition, reproduce the main features of the full nonlinear model in order to preserve the necessary balance between forecasts and analysis. The preliminary one dimensional studies, as in Chevalier et al, 2004, show that it is possible to select cloud-affected channels for which the accuracy and linearity of the observation operator are "acceptable" from a variational assimilation point of view. Even with a static bias correction and a conservative observation error specification, 1D-VAR assimilation results presented in Chevalier et al. 2004, are encouraging. In the present study the objective is to go one step further by trying to use AIRS cloudy radiances directly in 4D-Var. The observation operators used are simplified to reduce nonlinearities. A careful automatic selection is adopted to keep only observations in atmospheric conditions well modelled by our observation operators.

Two approaches are used to assimilate cloud-affected AIRS data. The first approach, detailed below, is based on a large scale cloud scheme combined with the RTTOVCLD. The second approach makes use of cloudy RTTOV with cloud top pressure and cloud cover coming from the CO2-slicing technique. Results from these two methods will provide

more elements to elaborate the strategy for the future use of cloudy radiances. To test the performance of the two approaches, four 4D-Var experiments are performed. The first experiment, henceforth called CLOUDDIAG, follows the diagnostic cloud scheme approach. The second experiment, henceforth called CLOUDCO2, was produced using the CO2-slicing cloud parameters. In the third experiment, henceforth called CLOUDCO21D, the CO2-slicing cloud parameters are adjusted by a prior 1D-VAR. The last control experiment, called CONTROL, was produced using only clear AIRS data. All experiments are conducted from 1 to 10 March 2004. At the beginning of this SAF mission, only 64 AIRS channels (see appendix 1) were used in the ARPEGE pre-operational data assimilation suite. Unfortunately bias correction coefficients are only calculated for this limited set of channels. All experiments exploit only the usable cloud-affected channels among this limited set.

4.1 CLOUDDIAG experiment

As stated above, the observation operator used in this approach consists of a combination of a simplified cloud scheme and a cloudy radiative transfer model (RTTOVCLD). The Tangent Linear (TL) and ADjoint (AD) versions of the cloud scheme have been developed in the framework of this study.

Within a screening step, a series of tests are performed to select usable AIRS cloud-affected FOVs/channels. Tests are sequenced as follows :

1. Only AIRS data over sea are used.
2. Perform, for each AIRS FOV, a cloud detection per channel using the ECMWF cloud detection scheme described in McNally and Watts, 2003 (see appendix 2). This scheme was previously implemented in 4D-Var to allow the assimilation of AIRS clear channels.
3. Verify, as described in section 3, if the FOV position is dominated by large scale cloudiness. If it is not the case the FOV is flagged nonusable and consequently only channels declared clear are used. This test is to ensure agreement with our large scale cloud scheme.
4. According to statistics, presented in section 3, only mid-latitudes FOVs are used (south of -40 and north of 40). For other regions only channels declared clear are used.
5. For each AIRS FOV, cloud top pressure and cloud cover are derived from the CO2-slicing algorithm.
6. Based on the associated cloud top pressure and on the linearity results (see Figure 9) a set of AIRS channels is attributed to each AIRS FOV depending on the cloud level. For selected channels, the observation operator has a linearity behaviour.
7. For the AIRS FOVs declared cloudy and for this first attempt, observation errors are simply derived from statistics shown in section 3.
8. For cloudy AIRS FOVs, only the channels having standard deviation of simulated minus observed TBs less than 5 K are used.

9. For the clear AIRS FOVs, observation errors must be inflated to take account of errors intrinsic to the cloud detection scheme. Indeed, even for clear sky the cloud scheme can generate a small amount of clouds.

For this first attempt to assimilate AIRS cloudy radiances and for the sake of simplicity we will use only FOVs with low clouds. The mean amount of AIRS channels, used in the minimisation, is nearly the same as in the control experiment. This can be explained by the fact that, in clear sky conditions, the number of usable channels is reduced to be in agreement with the new observation operator linearity requirements (see typical coverage example in Figure 10).

4.2 CLOUDCO2 experiment

Statistics presented in section 3 show that the CO₂-slicing technique combined with RTTOV can reduce significantly the departure between modelled and observed cloudy TBs. This reduction has a physical sense for channels peaking near the cloud top pressure. More investigations are necessary to understand the nature of resulted "innovations" for channels peaking lower in the atmosphere. Unphysical small "innovations" can comfort the analysis in its own bias. The use of the CTP and CC in RTTOV may introduce a correlation between the AIRS channels. This aspect is very important but the nature of introduced correlation is not well understood. Consequently no correlation is considered between used AIRS cloudy channels.

A criterion has to be defined to select the cloud-affected channels usable for the data assimilation. In this study we test a method based on the ECMWF cloud detection module. After a call, within the screening, of the observation operator, a rerun of the ECMWF cloud detection scheme is performed but without the ranking step (results of the previous run are used) and with the simulated cloudy spectrum instead of the clear one. This operation will, naturally, declare cloudy only channels having still important remaining cloud signal. Another criterion, envisaged in the future, could be to select the channels for which the residual errors in simulated cloud-affected channels are smaller than those induced by the standard errors of the background temperature and humidity profiles.

As in CLOUDIAG experiment, all decisions are taken within the screening step. Tests are sequenced as follows :

1. Only AIRS data over sea are used.
2. Perform, for each AIRS FOV, a cloud detection per channel using the ECMWF cloud detection scheme.
3. For each AIRS FOV, the cloud top pressure and cloud cover are derived from the CO₂-slicing algorithm. Cloud parameters are stored, in the observation file, for a subsequent use in the minimisation step.
4. Only FOVs with cloud cover between 0.3 and 0.99 are used. Dahoui et al, 2004 shows that the CO₂-slicing method is highly efficient for clouds covering more than 30 % of the FOV. When the cloud cover is equal to 1, the CO₂-slicing result is sometimes doubtful. Indeed, when the method detects the presence of cloud but makes a shift of the cloud top pressure, the resulting cloud cover may be more or equal to 1.

5. For the cloudy FOVs, the observation errors, associated to the cloud-affected channels are increased according to the results presented in section 3.
6. For the cloudy FOVs, the observation errors associated to clear channels, are inflated to deal with errors inherent to the CO2-slicing technique.

For technical reasons, the cloud top pressure and cloud cover are kept constant during the minimisation process. This constraint may limit the potential benefit of the method. The mean amount of AIRS channel, used in the minimisation, is around 26000 instead of 16000 in the control experiment (see typical coverage example in Figure 11).

4.3 CLOUDCO21D experiment

As stated in Dahoui et al, 2004, 11 % of the MODIS cloudy FOVs are not well detected by the CO2-slicing algorithm. 15 % of the MODIS cloud free FOVs are declared cloudy by this technique. The derived cloud top pressure has standard deviation errors around 100 hpa. The 1D-VAR scheme (see section 2) can adjust the CO2-slicing cloud parameters to be close to reality. It can help to decide in ambiguous cases such as in low cloudy conditions. Indeed, the CO2-slicing method has some difficulties to distinguish between very low cloudy and clear sky FOVs. In nearly all ambiguous cases, the 1D-VAR fails to retrieve a realistic cloud cover (between 0 and 1). In those cases, the FOV is simply flagged to be unusable and consequently only clear channels are used.

Statistics, presented in section 3, shows that the observation operator, with adjusted CO2-slicing cloud parameters, reduces significantly the departure between observed and simulated TBs. However, the risk is that the 1D-VAR can remove the useful information of the data and consequently comfort the analysis in its own bias.

In the framework of this study, the 1D-VAR code is outside the ARPEGE 4D-VAR system. Prior screenings are performed over the studied period using the operational analyses. For each screening network, we store all information necessary to run 1D-VAR (the background profiles, CO2-slicing results and observed TBs). The 1D-VAR adjusted cloud fields and associated flags are stored for further use by the CLOUDCO21D experiment.

The method used to select usable AIRS cloud-affected channels is the same as described in the CLOUDCO2 experiment.

4.4 Results

The impact on the forecast skill of 10 days assimilation of the AIRS cloudy radiances is examined by comparing the objective scores and by evaluating the fit of the forecasts to the observations (SYNOP and TEMP). Objective scores used in this study are the Root Mean Square (RMS) errors of atmospheric parameters averaged over the experiment period. The atmospheric parameters, used for the evaluation, are the geopotential, temperature, specific humidity and wind. The impact is evaluated over four synoptic domains : Europe, NH (North of 20 N), SH (South of 20 S) and Tropics.

4.4.1 CLOUDDIAG experiment

For all the parameters and for all domains, the synoptic impact of AIRS cloudy radiances, using the diagnostic cloud scheme, is slightly positive or neutral. This can be shown, at 500 hpa, by figures 12, 13, 14 and 15. The same results are obtained at nearly

all levels. A slight negative impact, on geopotential, is observed near 50 hpa in tropics (not shown). The fit to observations is also in favour of CLOUDDIAG as can be seen, for TEMP data, in figures 16, 17, 18 and 19. Although the improvements are marginal, results are very encouraging since observation errors were not specified optimally. In addition, criteria used to select usable cloud-affected channel are very stringent and consequently, they severely limit the number of channels used by the analysis.

The strategy for the future use of this method, is to investigate further observation error statistics, in the cloudy conditions, and then to establish optimal statistics. It is also necessary to review the bias correction philosophy in order to deal with cloudy radiances. One may add a correction term which depends on the cloud top pressure and the cloud cover. This will, even with a static correction term, help to remove an important part of the bias. More attention must be given to cloud-affected channel selection in order to use all useful channels. In the near future it is advised to keep the actual degree of simplicity and to continue working in large scale cloudiness conditions.

4.4.2 CLOUDCO2 experiment

The impact of using the crude CO₂-slicing cloud fields, directly in the analysis, is generally negative, except in the tropics where the impact is slightly positive. The negative impact is more pronounced, for all parameters, between 850 and 200 hpa. Figures 12, 13, 14 and 15 show that the negative impact is present at all the forecast ranges. The fit to the observations is not in favour of CLOUDCO₂ compared to the CONTROL experiment. Figures 20, 21, 22, 23 indicate that the fit to TEMP data gets worse with forecast range, especially between the surface and 200 hpa. In the tropics the fit to the observations is in favour of CLOUDCO₂.

The negative impact is generally moderate for all parameters. It can be attributed firstly to the shortcomings of the CO₂-slicing method in low cloudiness conditions. Secondly, the observation error statistics were not specified optimally ; Statistics for clear conditions are simply inflated by the same factor for all channels. The negative impact can, also, be caused by the fact that cloud top pressure and cloud cover were kept constant during the minimization. Certainly, the non use of correlations between cloud-affected channels is responsible for a part of this degradation.

4.4.3 CLOUDCO21D experiment

As expected, the use of a prior 1D-VAR adjustment of cloud fields, reduces significantly the negative impact of the method. The impact is negative in the Northern Hemisphere and slightly positive in the Tropics. In the Southern Hemisphere, the impact is negative between the surface and 500 hpa and positive elsewhere. As can be seen in Figures 24, 25, 26 and 27, the fit to observation is generally in favour of the CONTROL experiment except in the tropics.

The slight negative impact can be attributed to the methodology used to run the 1D-Var. Indeed, for technical reasons the 1D-Var runs are conducted outside the ARPEGE assimilation system. The used background fields are from the operational suite and not from the CLOUDCO₂1D experiment. A proper application of this approach is to call the 1D-VAR inside the ARPEGE screening module. As outlined above, the negative impact can also be attributed to the observation error statistics and the non use of correlations between cloudy channels.

The strategy for the future use of this method is to allow the adjustment of the cloud top

pressure and the cloud cover inside the analysis or, at least, run the 1D-VAR inside the screening module. More investigations of observation error statistics, in cloudy conditions, are necessary for an optimal use of cloudy radiances. Cloud-affected channels must be correlated. Finally, it is interesting to conduct similar experiments using AIRS cloudy radiances in the presence of medium and high clouds.

5 Conclusion

The main goal of this work was to assimilate AIRS radiances in cloudy conditions. Two approaches were used : the first approach is based on a combination of a large scale cloud scheme and RTTOVCLD to simulate AIRS cloudy radiances. The second approach makes use of the cloud top pressure and the cloud cover derived from the CO2-slicing technique. In a first stage, CO2-slicing outputs are directly used by RTTOV to simulate the cloud-affected spectrum. In a second stage, CO2-slicing outputs are adjusted by a prior 1D-VAR before being used by RTTOV. To prepare the 4D-VAR assimilation of AIRS cloudy radiances using these two approaches, the ARPEGE assimilation code was upgraded by the implementation of the CO2-slicing algorithm and by the revision of the observation operators. Before the assimilation experiments, the accuracy and linearity of the observation operators were investigated. The results were used to establish the selection criteria of cloud-affected channels. Derived error statistics were used, with conservative values, by the assimilation experiments.

To test the two assimilation approaches, four 4D-VAR experiments were conducted over a 10 day period. Results are in favour of the first approach. However, criteria (accuracy, linearity and cloud type) used to select usable cloud-affected channels limit severely the amount of channels used by the minimisation. Results are not in favour of the second approach, except in the Tropics. However, with the 1D-VAR adjusted cloud parameters, the negative impact is marginal.

As a first attempt, the results are encouraging. However, many aspects of the schemes need more investigation to improve the assimilation results. Then it will be necessary to review the bias correction in cloudy conditions. More attention must be given to the specification of the observation error statistics in the presence of clouds. The assimilation code must be upgraded to allow the adjustment, inside the screening module, of the CO2-slicing output cloud parameters.

The current implementation allows only the exclusive use of one of the two approaches. This limitation is imposed by the current observation distribution between processors. Indeed, the first approach requires RTTOVCLD and the second needs RTTOV. The observation packets supplied to the observation operator may contain observations usable only by one method. To allow the use of the two methods, criteria are needed, inside the screening, to affect each cloudy observation to one of the two methods. Then, observations must be redistributed between processors according to this affectation decision.

Acknowledgments

The authors would like to thank all CNRM/GMAP at Toulouse and CMS/R&D at Lannion for their support during this study. This work was supported by NWP-SAF sponsored by EUMETSAT.

References

- [1] Aumann, H.H. Chahine, M.T. Gautier, C. Goldberg, M.D. Kalnay, E. McMillin, L.M. Revercomb, H. Rosenkranz, P.W. Smith, W.L. Staelin, D.H. Strow, L.L. Susskind, J., 2003 : AIRS/AMSU/HSB on the Aqua mission: Design, science objectives, data products and processing systems. IEEE transaction on geoscience and remote sensing, VOL. **41**, NO. 2, 253-264.
- [2] Auligné, T., Rabier, F., 2004 : Assimilation results for AIRS at Météo-France. Proceedings of the ECMWF Workshop on Assimilation of high spectral resolution sounders in NWP, 28 june - 1 july 2004.
- [3] Chevalier F., Lopez P., Tompkins A., Janisková M. and Moreau E., 2004 : The capability of 4D-Var systems to assimilate cloud-affected satellite infrared radiances. Q. J. R. Meteorol. Soc, **130**, 917-932.
- [4] Dahoui. M., Lavanant. L., Rabier. F., Auligné. T., 2004 : Use of MODIS imager to help dealing with AIRS cloudy radiances. Q. J. R. Meteorol. Soc, in revision.
- [5] Eyre. J. R., 1992 : A bias correction scheme for simulated TOVS brightness temperatures. ECMWF Technical Memorandum No. 186 (available from ECMWF).
- [6] Fourrié, N. and Rabier, F., 2003 : Cloud characteristics and channel selection for IASI radiances in meteorologically sensitive areas. Q. J. R. Meteorol. Soc, **130**, 1839-1856.
- [7] Gilbert, J. C. and Lemaréchal, C., 1989: Some numerical experiments with variable-storage quasi-Newton algorithms. Math. Programming, **45**, 407-435.
- [8] Gérard, L., 2001 : Physical Parametrizations in ARPÈGE-ALADIN operational model. Météo France internal documentation.
- [9] Harris, B. A., and Kelly, G., 2001 : A satellite radiance bias correction scheme for radiance assimilation. Q. J. R. Meteorol. Soc, **127**, 1453-1468.
- [10] Janisková, M., Mahfouf, J. F. and Morcrette, J. J., 2002 : Preliminary studies on the variational assimilation of cloud-radiation observations. Q. J. R. Meteorol. Soc, **128**, 2713-2736.
- [11] Lavanant. L, 2002 : Cloud processins in IASI context. ITSC12 proceedings.
- [12] McNally, A. P. and P. D. Watts, 2003: A cloud detection algorithm for high spectral resolution infrared sounders. Q. J. Roy. Meteorol. Soc., **129**, 3411-3423.
- [13] McNally, A. P., 2002 : A note on the occurence of cloud in meteorologically sensitive areas and the implications for advanced infrared sounders. Q. J. R. Meteorol. Soc, **128**, 2551-2556.
- [14] Menzel, W. Smith, T. Stewart., 1983 : Improved cloud motion wind vector and altitude assignment using VAS. J. Applied Meteorology., **22**, 377-384.
- [15] Phulpin, T., Cayla, F., Chalon, G., Diebel, D. and D. Schluessel, 2002 : IASI onboard Metop : Project status and scientific preparation. Proceedings of the 12th International TOVS Study Conference, 26/02 to 4/03/2002, Australia.

- [16] Platnick, S., M. D. King, S. A. Ackerman, W. P. Menzel, B. A. Baum, C. Riedl, and R. A. Frey, 2003 : The MODIS cloud products: Algorithms and examples from Terra. IEEE Transactions on Geoscience and Remote Sensing, Aqua Special, VOL. **41**, NO. 2, 459-473.
- [17] Rabier, F., Järvinen, H., Klinker, E., Mahfouf, J.-F and Simmons, A., 2000 : The ECMWF operational implementation of four dimensional variational assimilation. Part I : Experimental results with simplified physics. Q. J. R. Meteorol. Soc, 1143-1170.
- [18] Saunders, R. W., P. Brunel, F. Chevallier, G. Deblonde, S. J. English, M. Matricardi and P. J. Rayer, 2002 : RTTOV-7 Science and Validation Report. NWP Forecasting Research Tech. Rep., 387.
- [19] SAF-NWC, 2002 : User Manual for the PGE01-02-03 of the SAFNWC/MSG : Scientific part. Eumetsat documentation.
- [20] Xu and Randall, 1996 : A semiempirical cloudiness Parametrization for use in climate models. Journal of the atmospheric sciences, Vol **53**. No 21:3084-3101.

Appendix 1

AIRS channel	wavenumber (cm^{-1})	wavelength (μm)
325	743.450989	13.4507856
333	745.992981	13.4049520
338	747.578003	13.3765306
355	753.028015	13.2797184
362	755.299011	13.2397900
375	759.546997	13.1657419
453	793.138977	12.6081305
475	801.067993	12.4833345
484	804.346008	12.4324598
497	809.142029	12.3587694
528	820.799011	12.1832514
587	843.875977	11.8500824
672	871.257019	11.4776697
787	917.270020	10.9019156
791	918.710022	10.8848276
843	937.864990	10.6625156
870	948.143005	10.5469322
1301	1236.57996	8.08682060
1329	1251.39001	7.99111366
1371	1285.43005	7.77949762
1415	1310.71997	7.62939453
1424	1316.01001	7.59872675
1449	1330.93005	7.51354265
1455	1334.55005	7.49316263
1466	1339.64001	7.46469212
1477	1345.26001	7.43350697
1479	1346.29004	7.42781973
1488	1351.02002	7.40181494
1500	1357.18005	7.36821890
1519	1367.20996	7.31416559
1520	1367.73999	7.31133080
1538	1377.37000	7.26021338
1545	1381.16003	7.24029064

Table 1: Set of AIRS channels used in the 4D-VAR (to be continued ...)

AIRS channel	wavenumber (cm^{-1})	wavelength (μm)
1565	1392.10999	7.18334055
1574	1397.07996	7.15778685
1583	1402.09998	7.13215923
1593	1407.70996	7.10373640
1627	1427.18005	7.00682449
1636	1432.40002	6.98128986
1652	1441.82996	6.93563080
1669	1468.79004	6.80832481
1694	1484.32996	6.73704672
1708	1493.17004	6.69716120
1723	1502.76001	6.65442276
1740	1513.78003	6.60597992
1748	1519.02002	6.58319139
1756	1524.30005	6.56038809
1766	1544.43005	6.47488070
1771	1547.82996	6.46065807
1777	1551.93994	6.44354868
1783	1556.05005	6.42652845
1794	1563.66003	6.39525175
1800	1567.83997	6.37820244
1806	1572.04004	6.36116123
1826	1586.20996	6.30433559
1843	1598.43994	6.25610018
1852	1604.98999	6.23056841
1865	2181.37988	4.58425426
1866	2182.27002	4.58238459
1868	2184.10010	4.57854462
1869	2185.00000	4.57665920
1872	2187.72998	4.57094812
1873	2188.63989	4.56904745
1875	2190.44995	4.56527185
1876	2191.37988	4.56333494
1877	2192.30005	4.56141949
1881	2195.96997	4.55379629
1882	2196.86011	4.55195093
1897	2210.71997	4.52341318
1901	2214.42993	4.51583481
1911	2223.82007	4.49676657
1917	2229.45996	4.48539114
1918	2230.39990	4.48350096
1921	2233.27002	4.47773886
1923	2235.12988	4.47401285
1924	2236.07007	4.47213173
1928	2239.89990	4.46448517

Appendix 2

ECMWF cloud detection scheme

The ECMWF scheme (McNally and Watts, 2003) aims to detect channels affected by clouds. Unaffected channels are potentially useful for the data assimilation system. The scheme makes use of simulated radiances and observed brightness temperatures. It performs the detection in several steps as follows :

- Simulated AIRS brightness temperatures are generated using the nearest NWP forecast profile and the RTTOV-7 forward model. Bias correction is applied to each channel.
- Each channel is assigned to the lowest level P_i (in RTTOV coordinates) at which the radiation effect of one layer opaque cloud at P_i , defined as $\frac{|R_{clear} - R_{cl}^{P_i}|}{R_{clear}}$, is less than 1%. R_{clear} denotes the simulated clear radiance and $R_{cl}^{P_i}$ the simulated black-body radiance at the cloud level P_i . The measured minus simulated brightness temperatures are then sorted according to the assigned level into five spectral bands namely $15 \mu m$, $9 \mu m$, $6 \mu m$, $4.5 \mu m$ and $4.2 \mu m$,
- A low pass filter is applied on the ranked information in order to smooth the instrument noise and the cloud emissivity effect.
- In each band, starting from the low peaking channel, the first position for which the gradient of the filtered observation minus model value is less than a predefined threshold, is considered as the end of cloud signal. all channels ranked above are flagged cloud free.

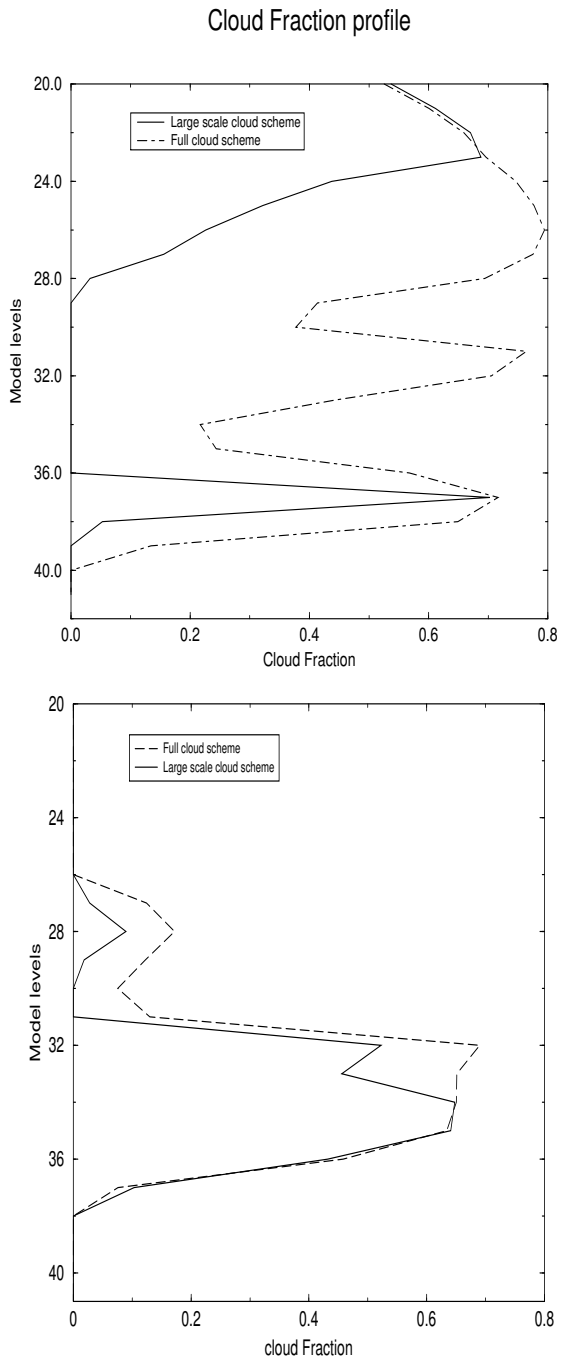


Figure 1: Typical examples of cloud fraction profiles generated by the large scale and the full diagnostic cloud schemes. In the top panel, the large difference between the two profiles indicates the presence of active convection processes. In bottom panel, the two profiles have the same shape and therefore, the pixel is considered as dominated by large scale cloudiness.

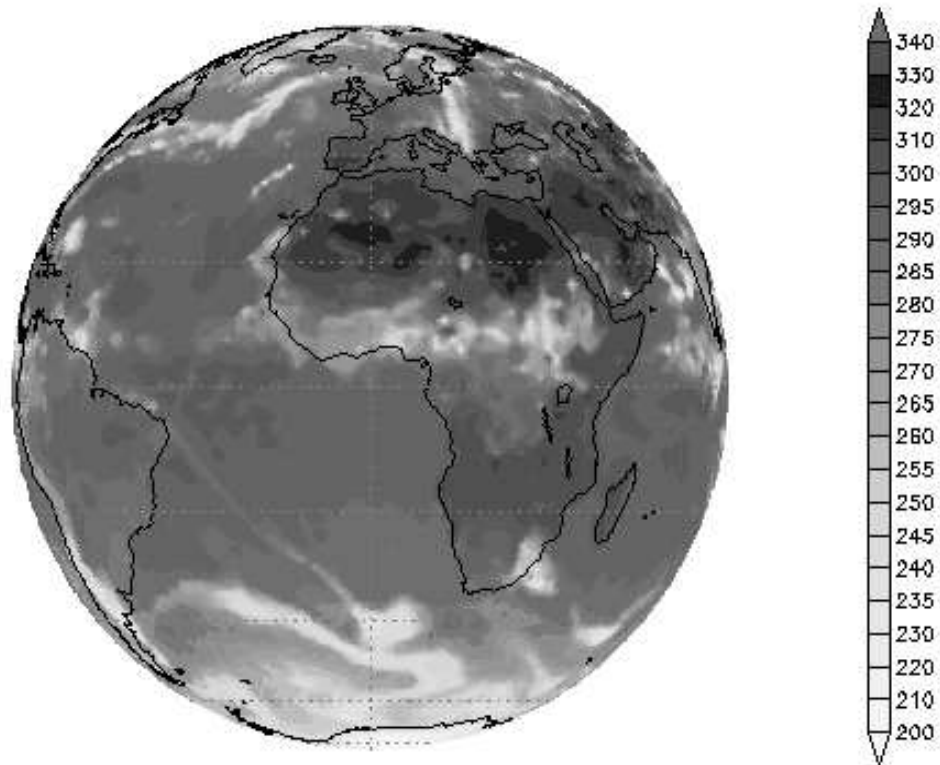
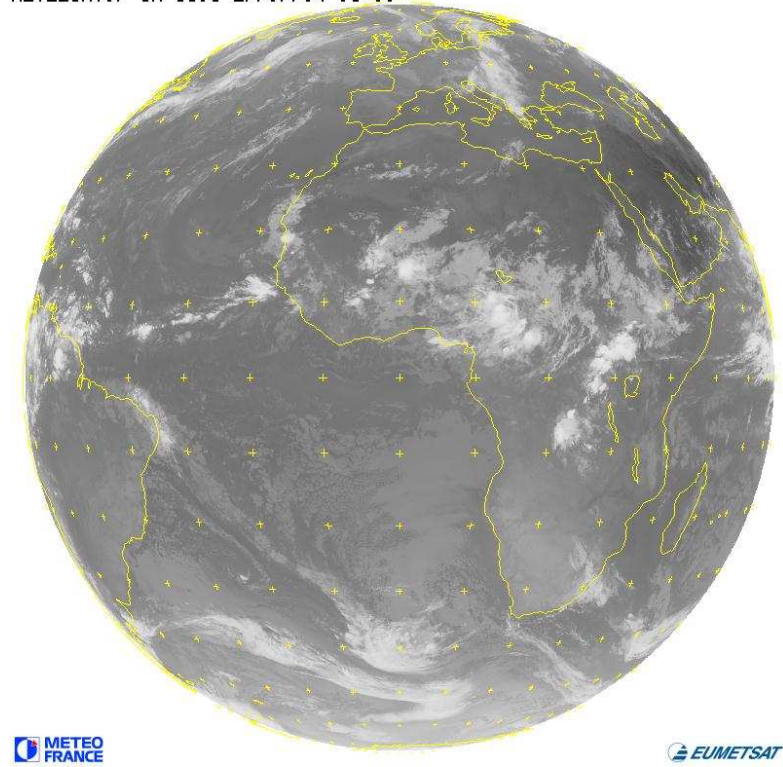


Figure 2: Observed (top) and simulated (bottom) Meteosat-7 11.5 μm at 06 UTC 27 June 2004. The grey scale is not the same between the two images.

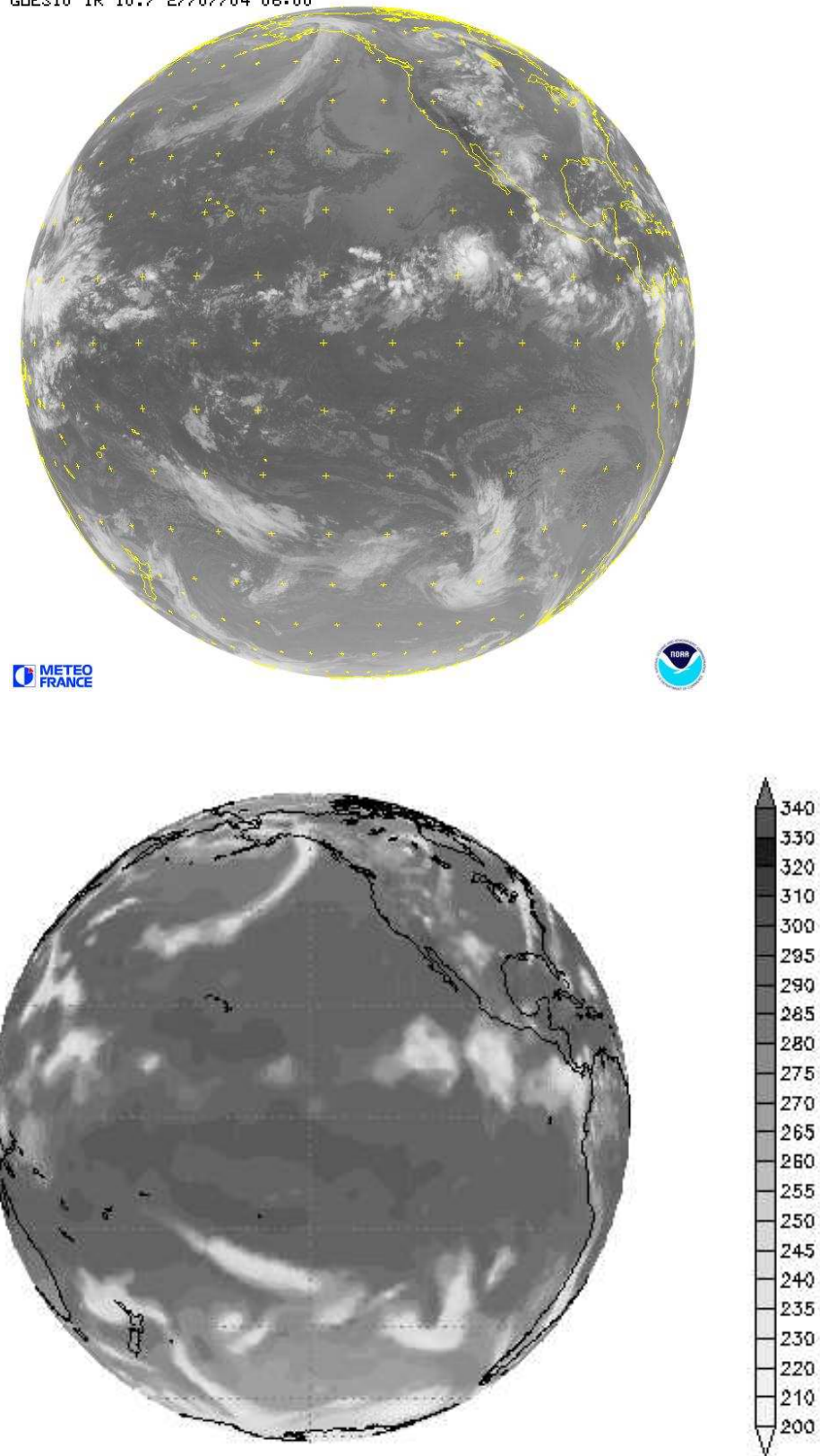


Figure 3: Observed (top) and simulated (bottom) GOES-10 10.7 μm at 06 UTC 27 June 2004. The grey scale is not the same between the two images.

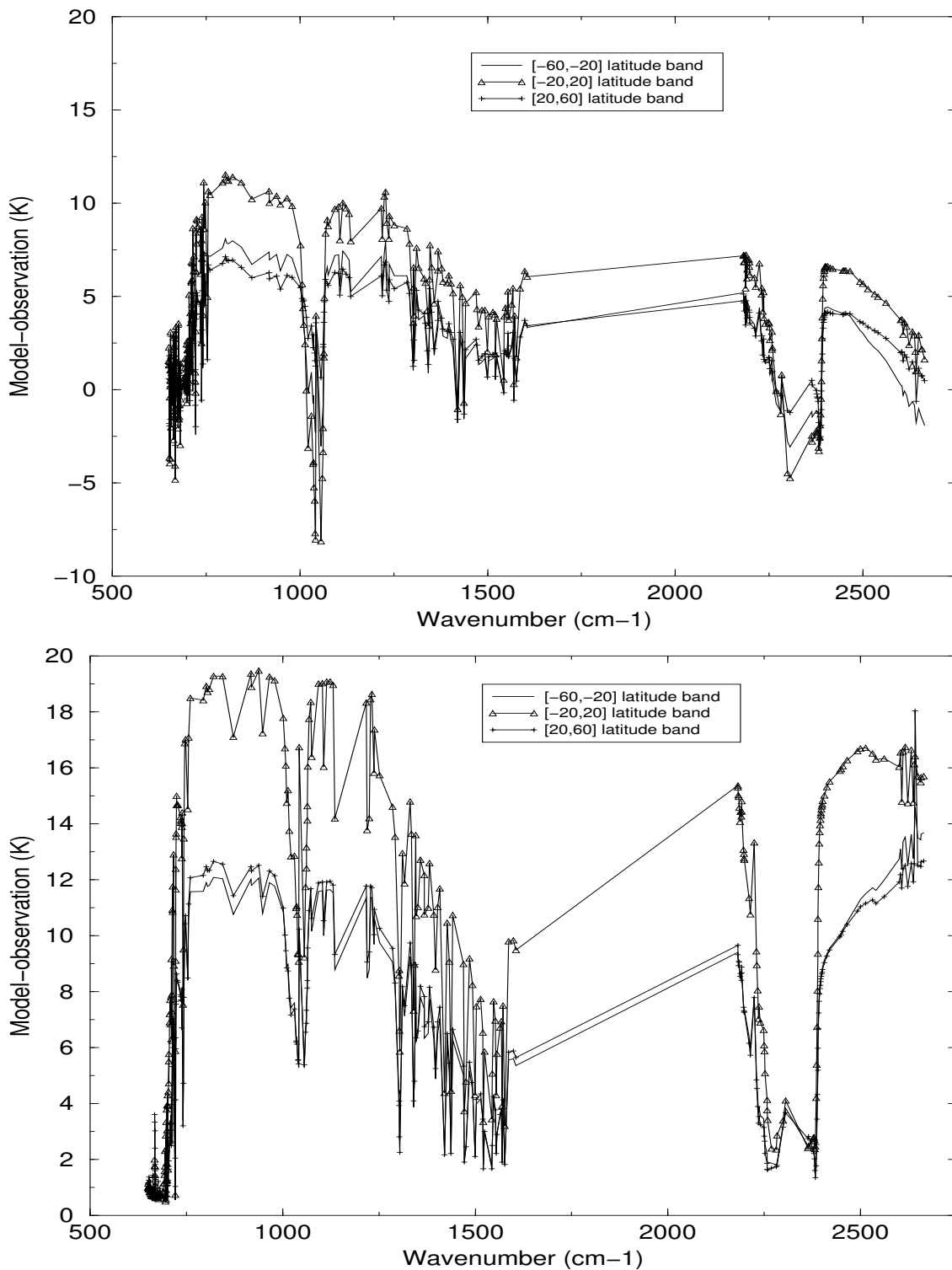


Figure 4: Bias (top) and standard deviation (bottom) of the differences between the simulated and the measured cloudy brightness temperatures averaged over various latitude bands. Cloud fields are produced using the operational ARPEGE cloud scheme. Statistics are for the period between 1 to 4 March 2004. Statistics over the second period are similar.

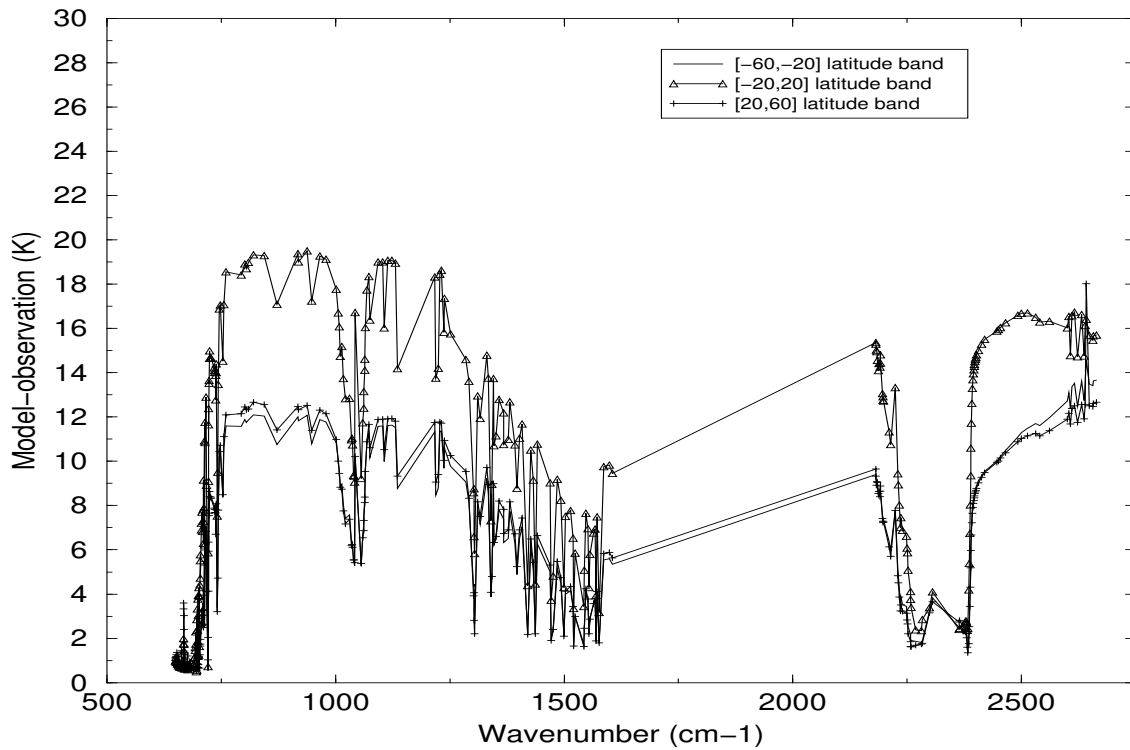
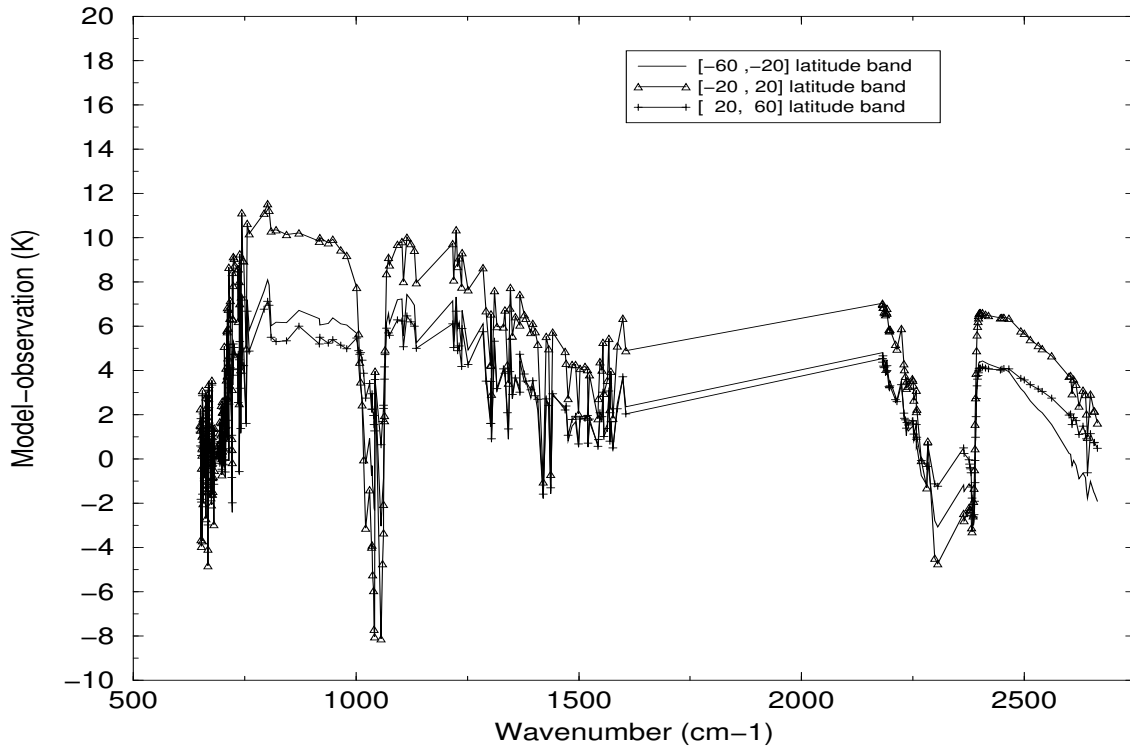


Figure 5: Bias (top) and standard deviation (bottom) of the differences between the simulated and the measured cloudy brightness temperatures averaged over various latitude bands. Cloud fields are produced using the large scale cloud scheme. Statistics are for the period between 1 to 4 March 2004. Statistics over the second period are similar.

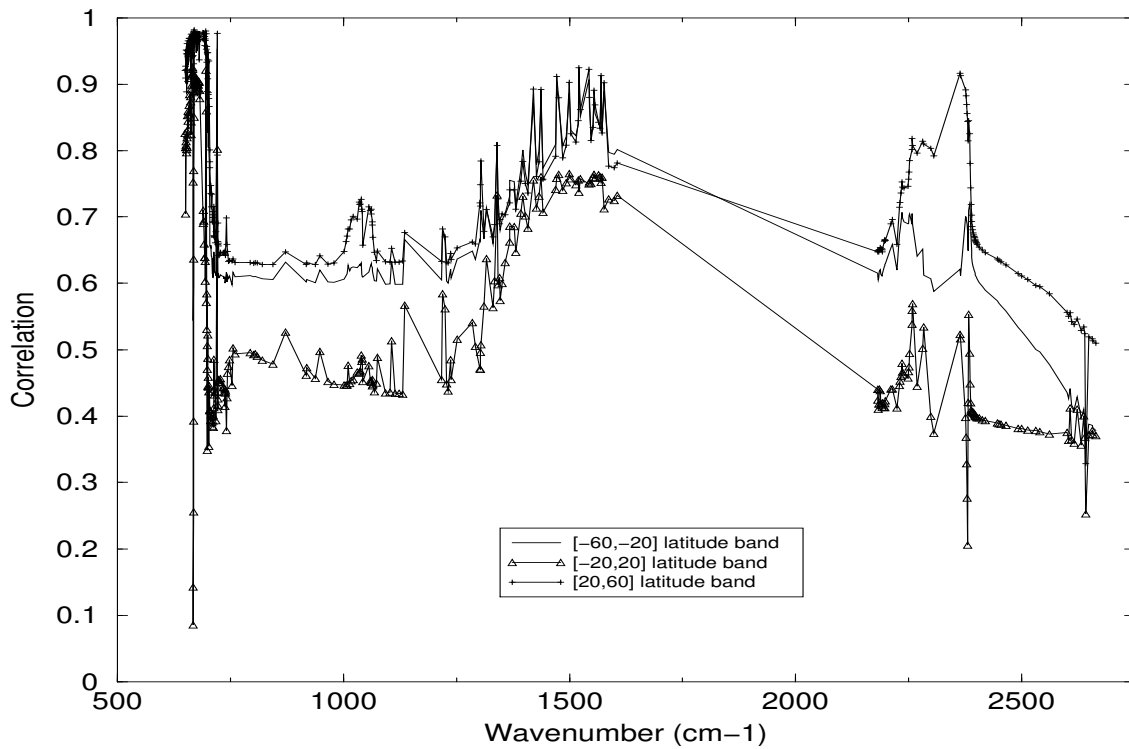


Figure 6: Spatial correlation between simulated and measured AIRS cloudy brightness temperatures using the large scale cloud scheme. Statistics are for the period between 1 to 4 March 2004.

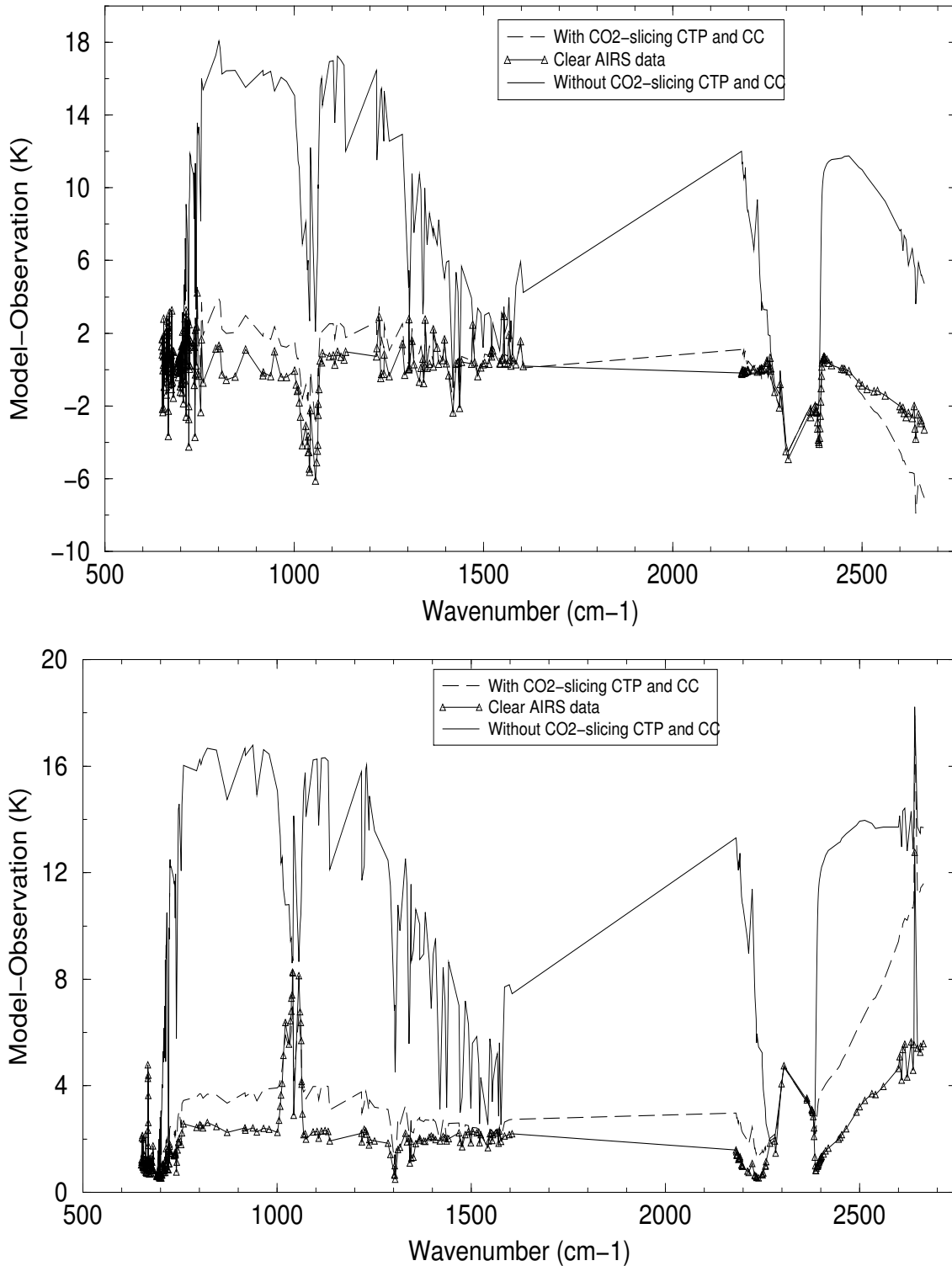


Figure 7: Bias (top) and standard deviation (bottom) of the departure between simulated and observed AIRS brightness temperatures in cloudy conditions. Simulated cloudy TBs are produced using RTTOV6 and cloud fields from the CO2-slicing algorithm. Statistics in clear conditions and statistics in cloudy conditions without using cloud fields are also shown.

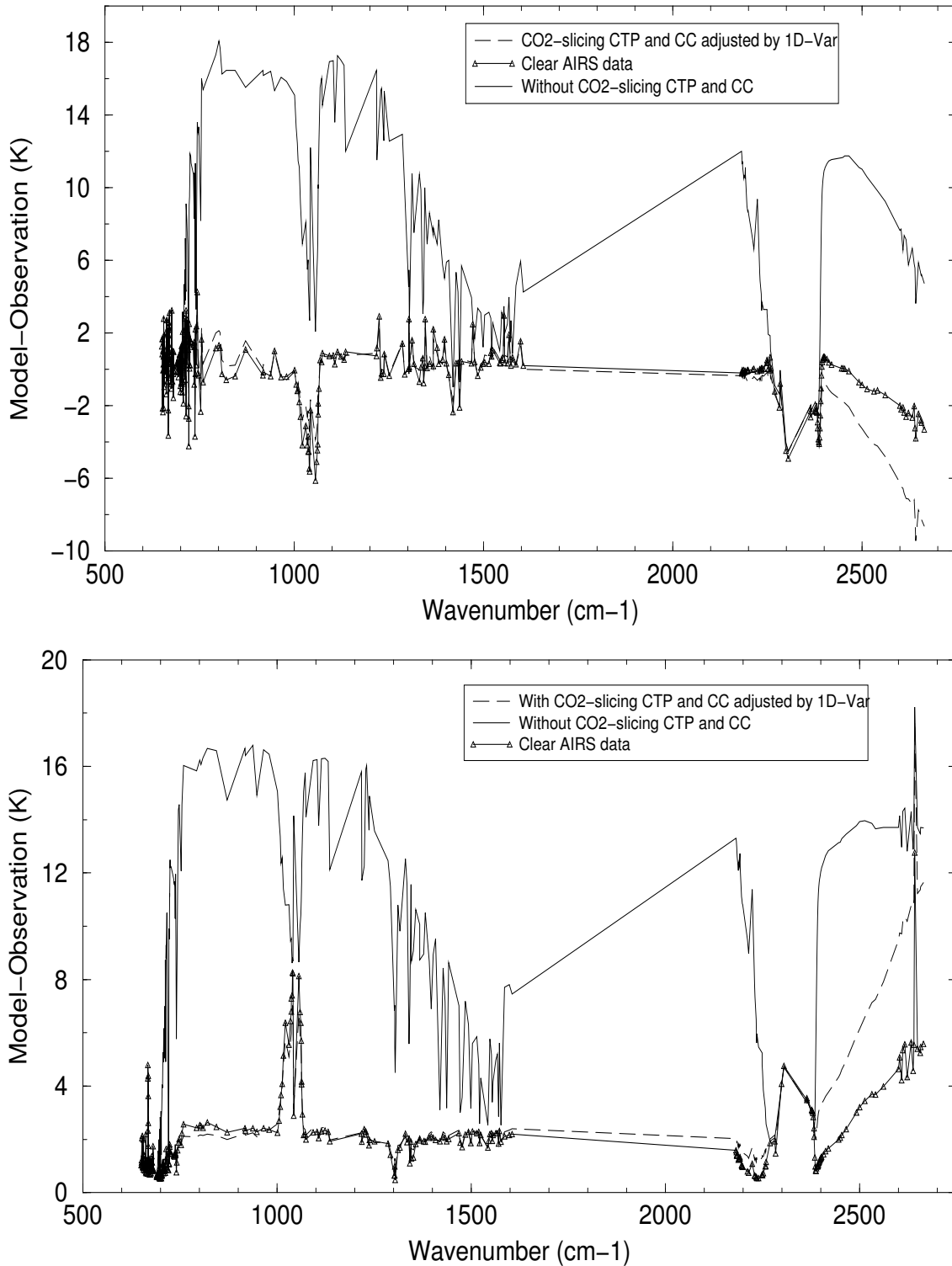


Figure 8: Bias (top) and standard deviation (bottom) of the departure between simulated and observed AIRS brightness temperatures in cloudy conditions. Simulated cloudy TBs are produced using RTTOV6 and 1D-VAR adjusted CO2-slicing cloud fields. Are also shown statistics in clear conditions and statistics in cloudy conditions without using cloud fields.

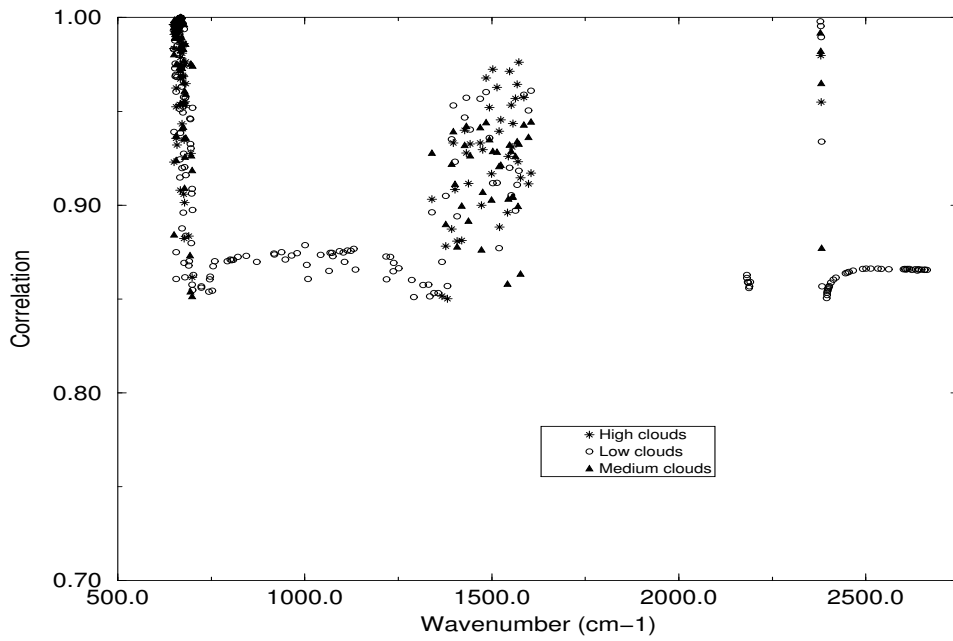
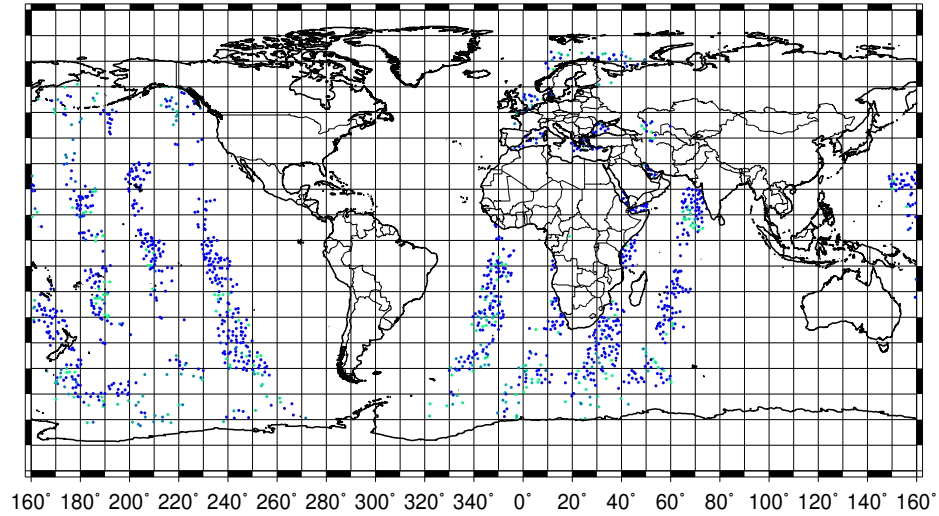
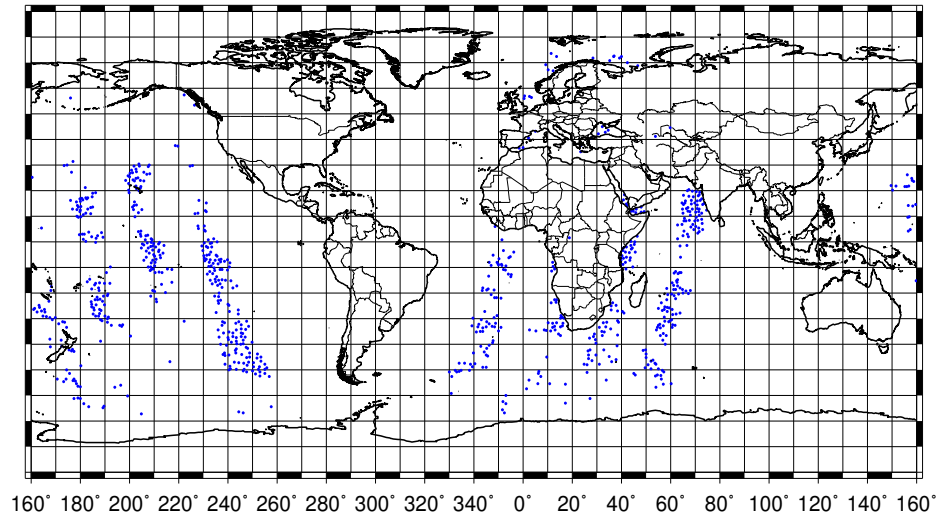


Figure 9: AIRS channels verifying the linearity assumption of the observation operator for different cloud types (correlations > 0.85).

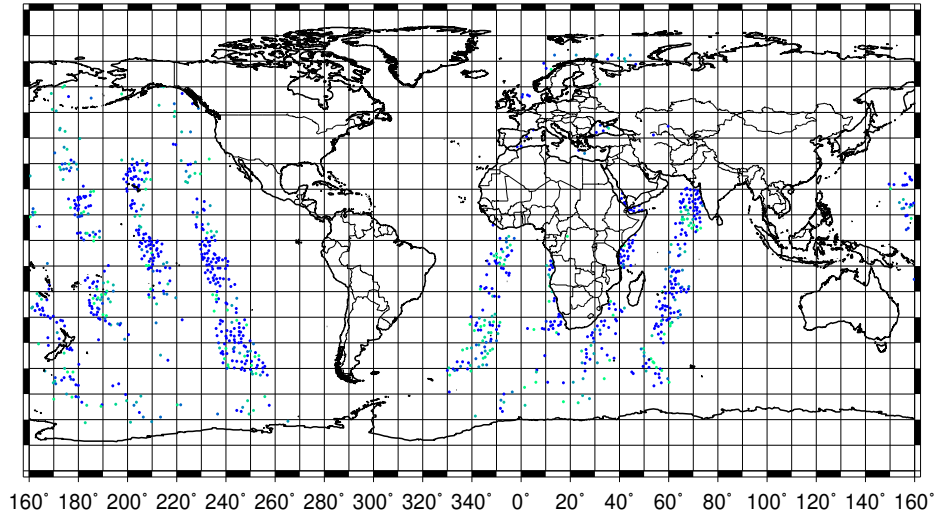


GMT 2004 Dec 28 13:41:13

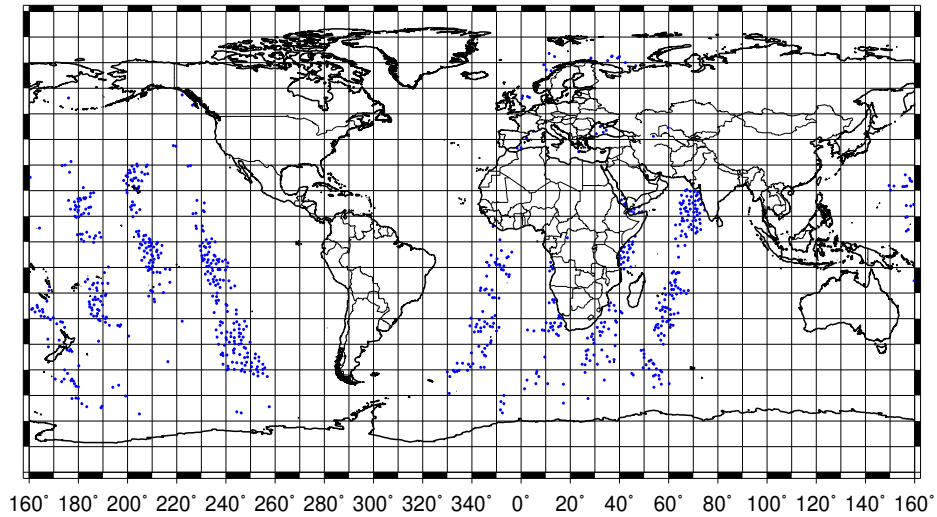


GMT 2004 Dec 28 13:45:13

Figure 10: Typical example of the AIRS channel 1502.76 cm^{-1} coverage used by the minimisation process in the CLOUDDIAG experiment (top) and in the CONTROL experiment (bottom). Clear and cloudy FOVs are, respectively, in blue and green.



GMT 2004 Dec 28 13:44:26



GMT 2004 Dec 28 13:45:13

Figure 11: Typical example of the AIRS channel 1502.76 cm^{-1} coverage used by the minimisation process in the CLOUDCO2 experiment (top) and in the CONTROL experiment (bottom). Clear and cloudy FOVs are, respectively, in blue and green.

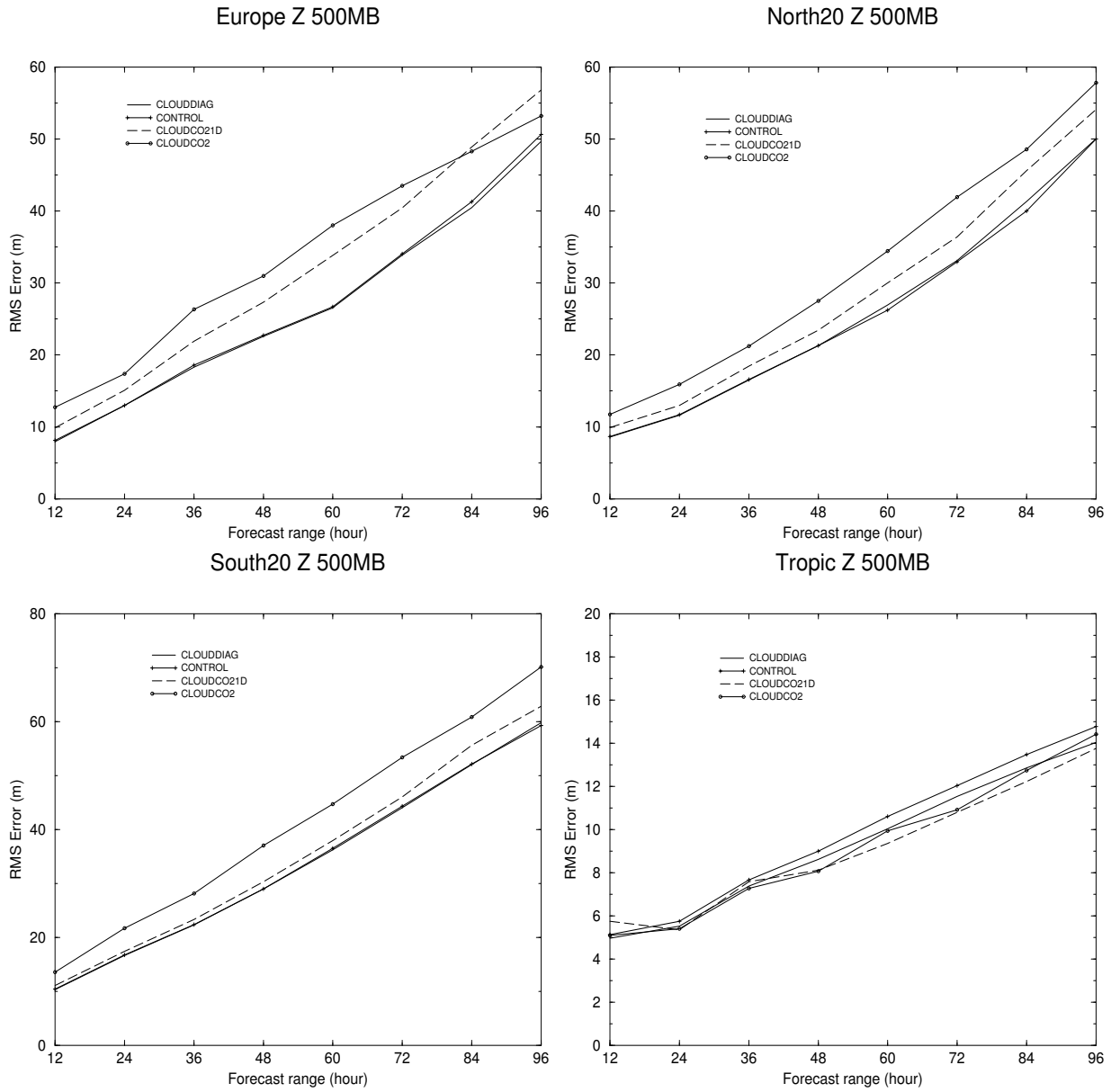


Figure 12: Root Mean Square (RMS) of geopotential errors for 4 days forecasts from CLOUDDIAG, CONTROL, CLOUDCO2 and CLOUDCO21D experiments. Results are averaged over 10 forecasts (01 to 10 March 2004). Forecasts are compared to their own analysis.

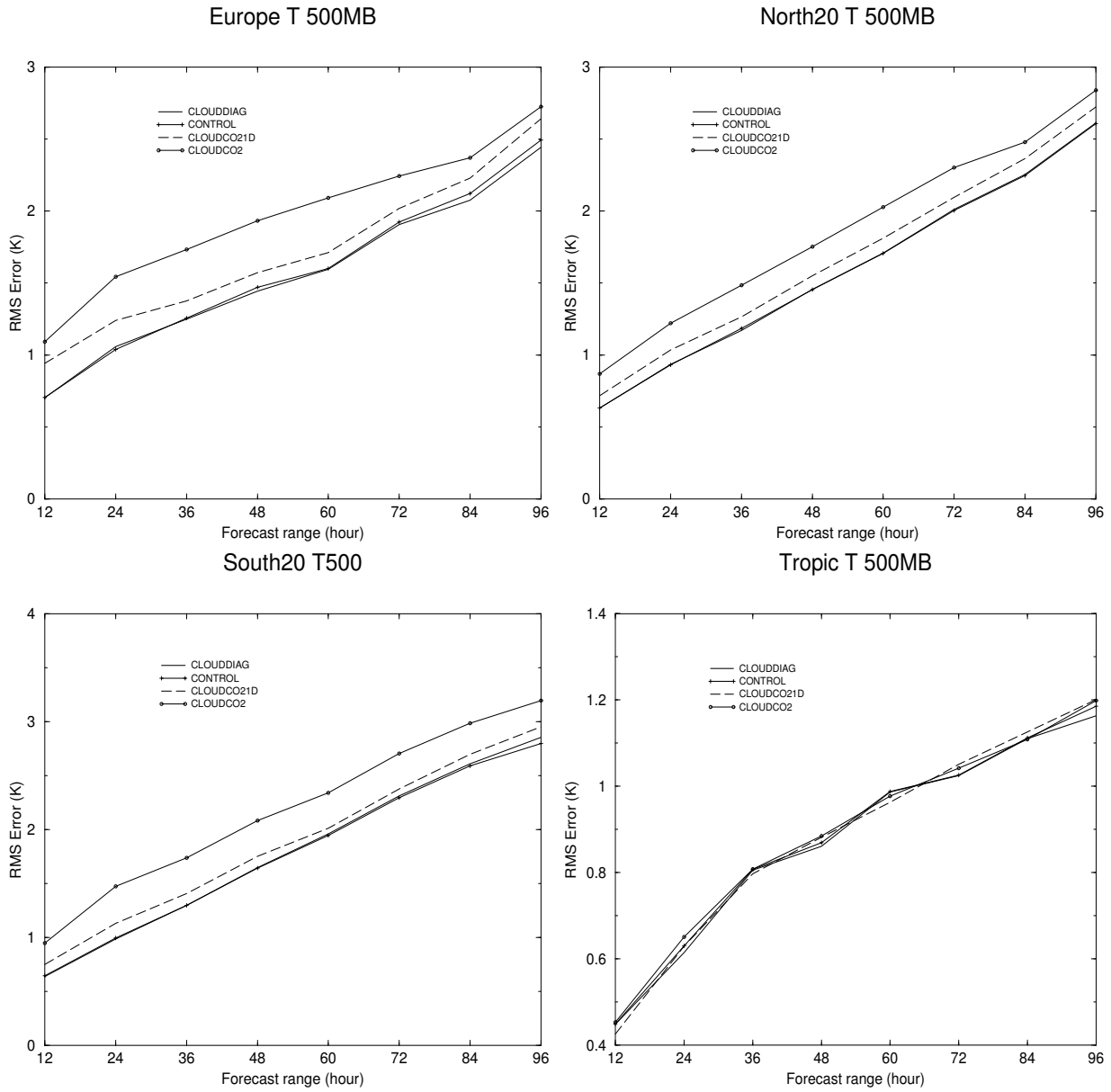


Figure 13: Root Mean Square (RMS) of temperature errors for 4 days forecasts from CLOUDDIAG, CONTROL, CLOUDCO2 and CLOUDCO21D experiments. Results are averaged over 10 forecasts (01 to 10 March 2004). Forecasts are compared to their own analysis.

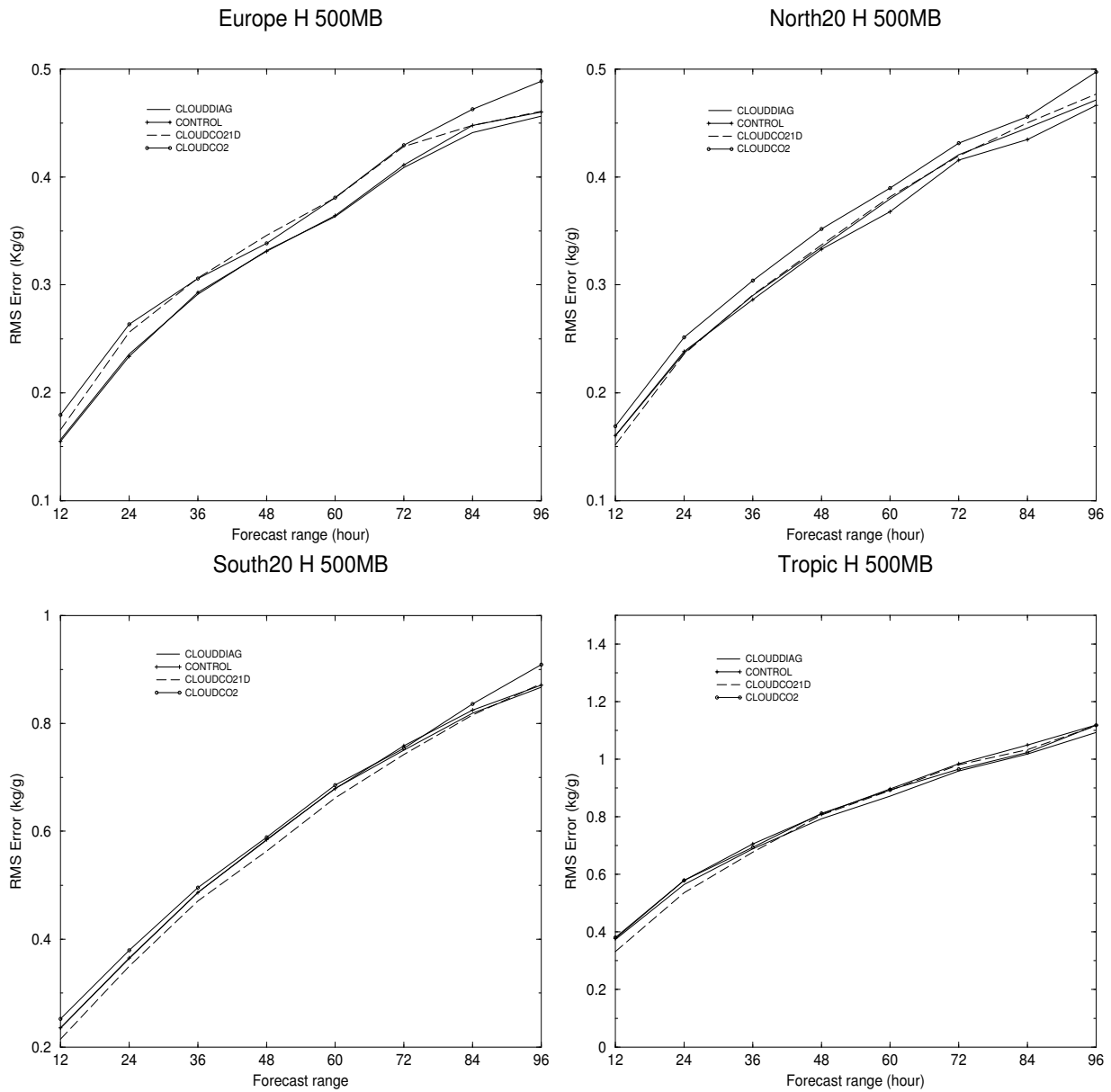


Figure 14: Root Mean Square (RMS) of specific humidity errors for 4 days forecasts from CLOUDDIAG, CONTROL, CLOUDCO2 and CLOUDCO21D experiments. Results are averaged over 10 forecasts (01 to 10 March 2004). Forecasts are compared to their own analysis.

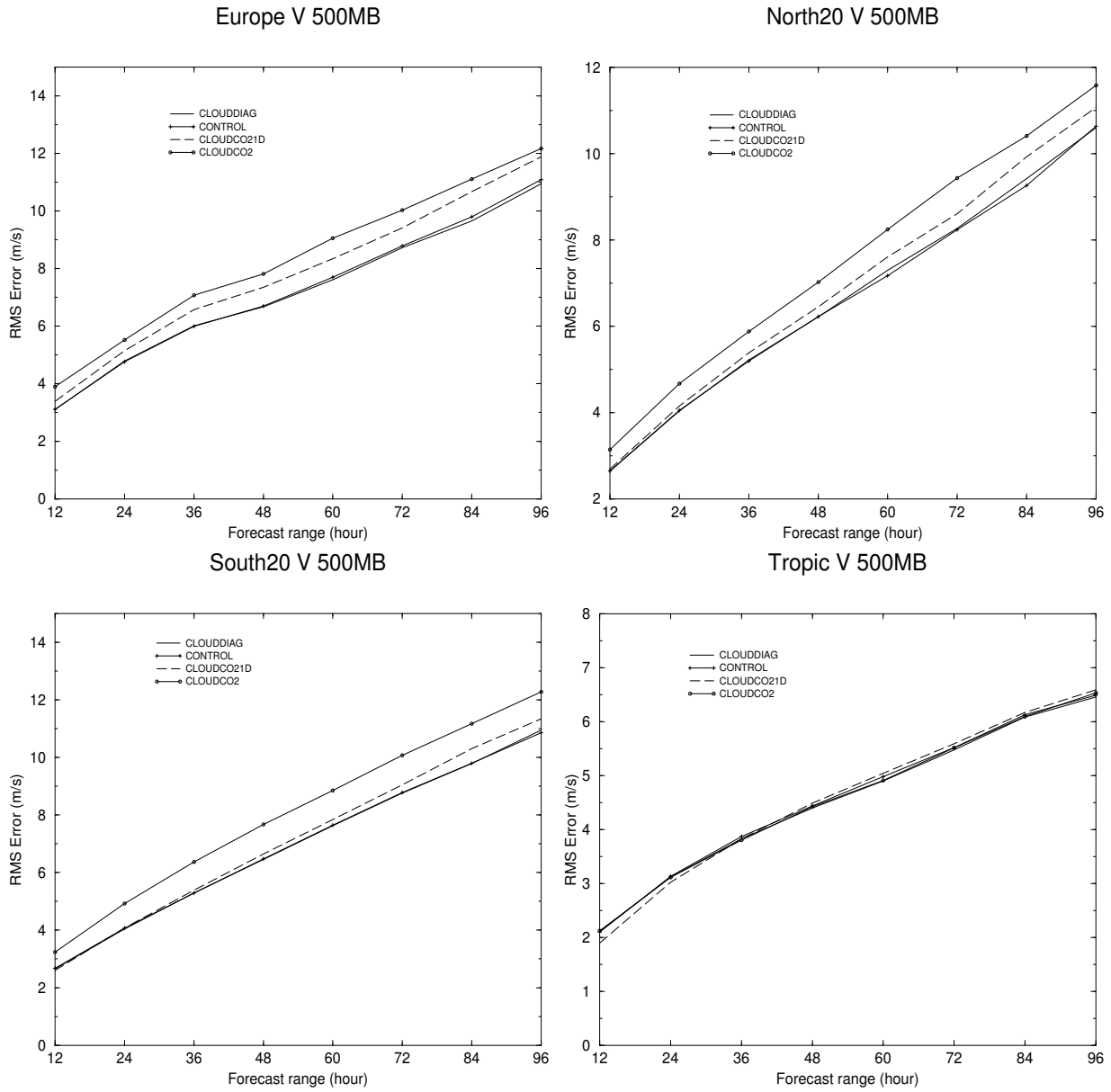


Figure 15: Root Mean Square (RMS) of wind errors for 4 days forecasts from CLOUDDIAG, CONTROL, CLOUDCO2 and CLOUDCO21D experiments. Results are averaged over 10 forecasts (01 to 10 March 2004). Forecasts are compared to their own analysis.

GEOPOTENTIEL

ECH. : / 24 / 48 / 72 /

9 cas, 01/03/2004_00UTC -> 13/03/2004_12UTC

— Biais P701I.r 0/TP

— Eqm P701I.r 0/TP

- - - Biais P700Z.r 0/TP

* - - * Eqm P700Z.r 0/TP

ECH.24

ECH.48

ECH.72

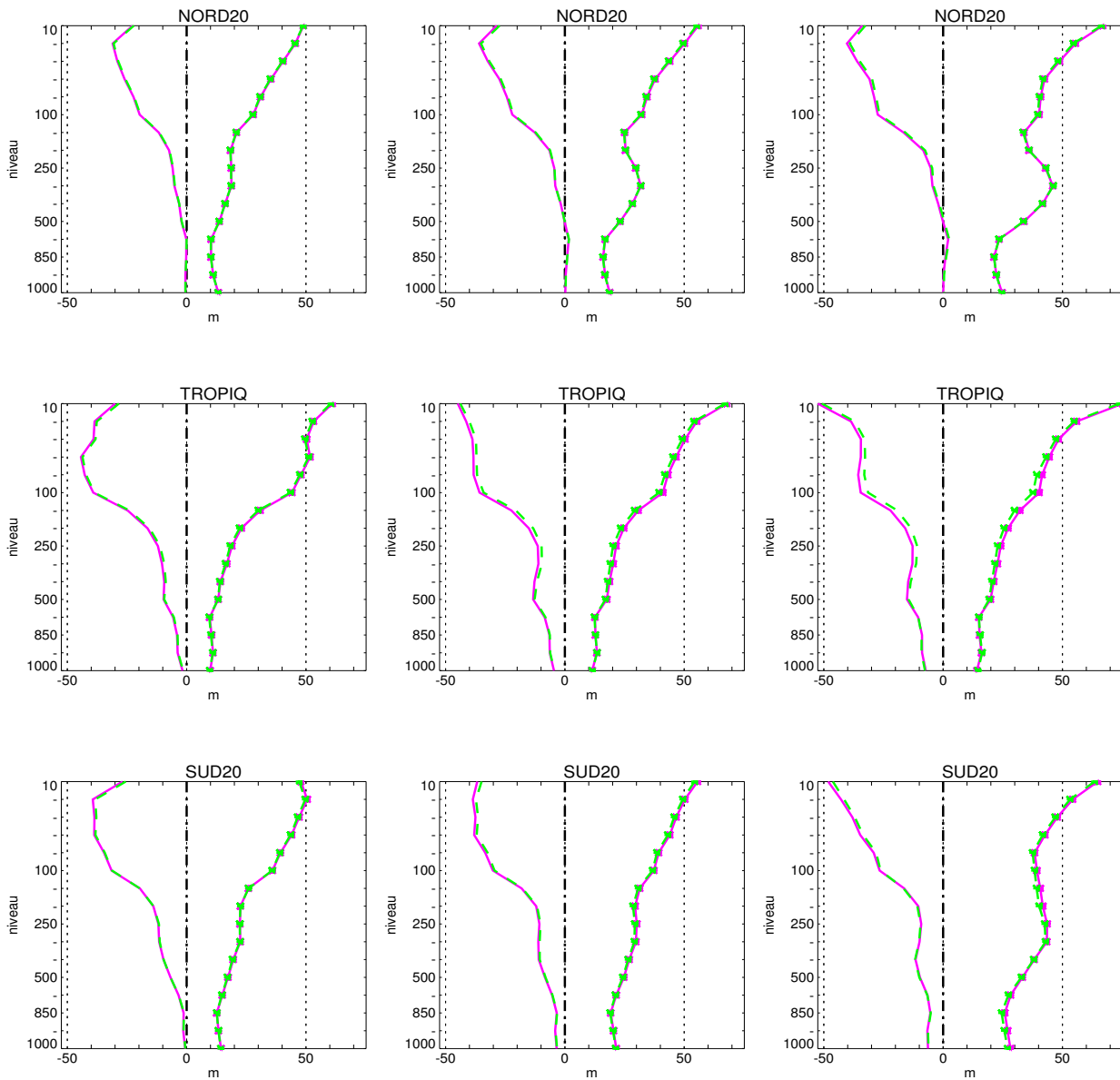


Figure 16: RMS and bias of geopotential errors from CLOUDDIAG (green) and CONTROL (magenta) experiments. Forecasts are compared to TEMP data. Results are averaged over 10 forecasts (01 to 10 March 2004).

TEMPERATURE

ECH. : / 24 / 48 / 72 /

9 cas, 01/03/2004_00UTC -> 13/03/2004_12UTC

— Biais P701I.r 0/TP

— Eqm P701I.r 0/TP

- - - Biais P700Z.r 0/TP

* - - * Eqm P700Z.r 0/TP

ECH.24

ECH.48

ECH.72

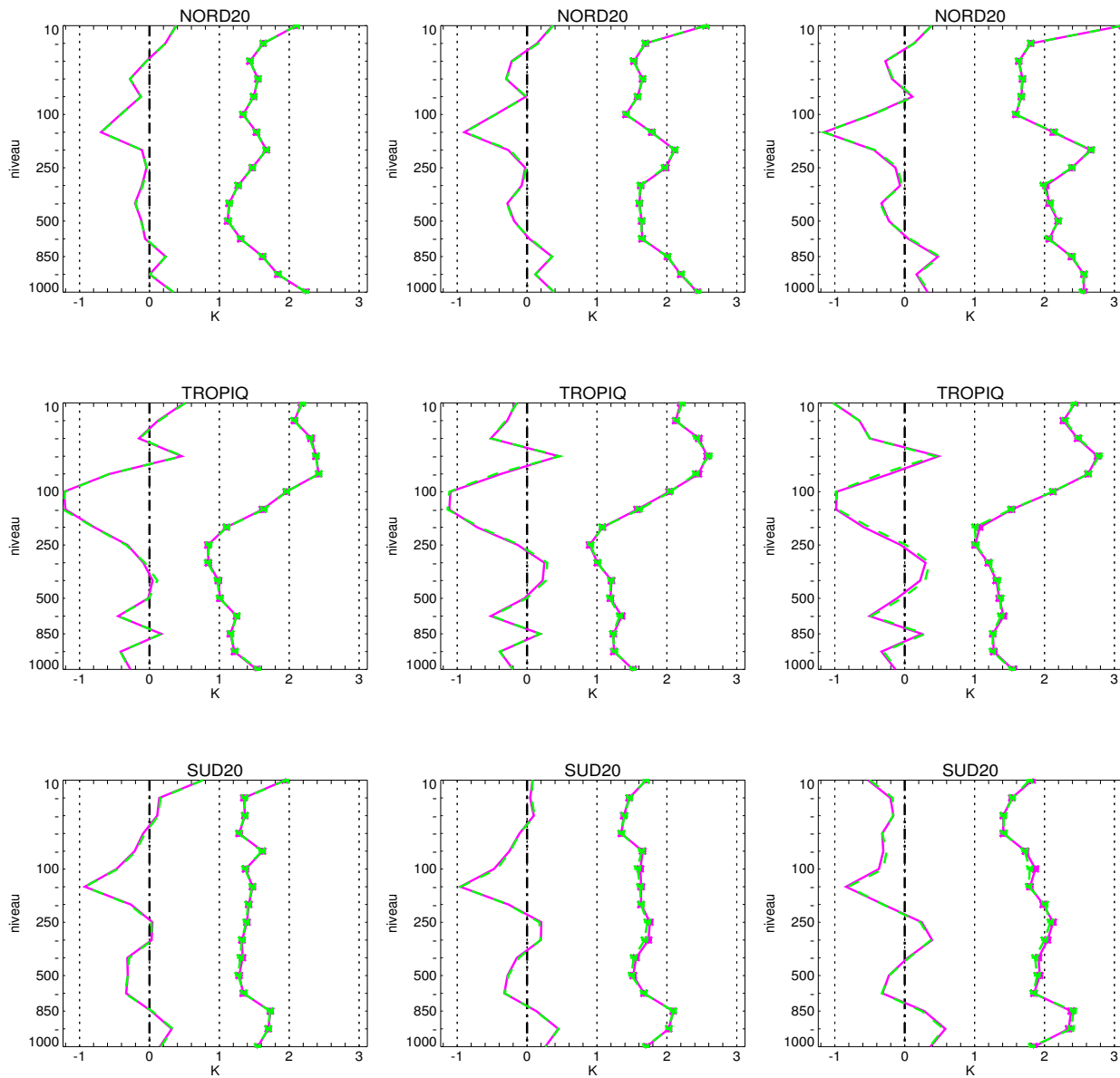


Figure 17: RMS and bias of temperature errors from CLOUDDIAG (green) and CONTROL (magenta) experiments. Forecasts are compared to TEMP data. Results are averaged over 10 forecasts (01 to 10 March 2004).

HUMIDITE

ECH. : / 24 / 48 / 72 /

9 cas, 01/03/2004_00UTC -> 13/03/2004_12UTC

— Biais P701I.r 0/TP

— Eqm P701I.r 0/TP

- - - Biais P700Z.r 0/TP

* - - * Eqm P700Z.r 0/TP

ECH.24

ECH.48

ECH.72

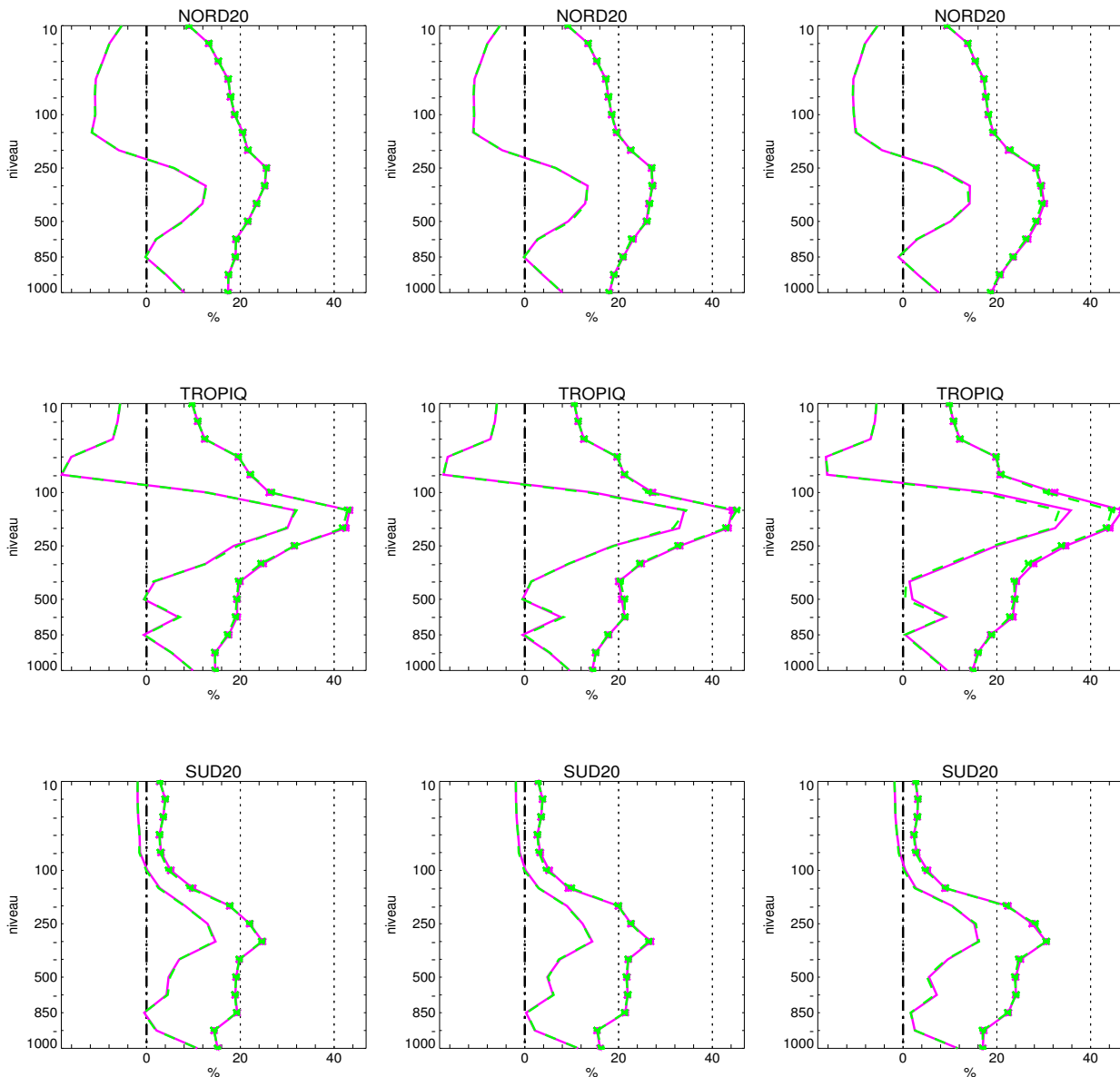


Figure 18: RMS and bias of humidity errors from CLOUDDIAG (green) and CONTROL (magenta) experiments. Forecasts are compared to TEMP data. Results are averaged over 10 forecasts (01 to 10 March 2004).

VENT

ECH. : / 24 / 48 / 72 /

9 cas, 01/03/2004_00UTC -> 13/03/2004_12UTC

— Biais P701I.r 0/TP

— Eqm P701I.r 0/TP

- - - Biais P700Z.r 0/TP

* - - * Eqm P700Z.r 0/TP

ECH.24

ECH.48

ECH.72

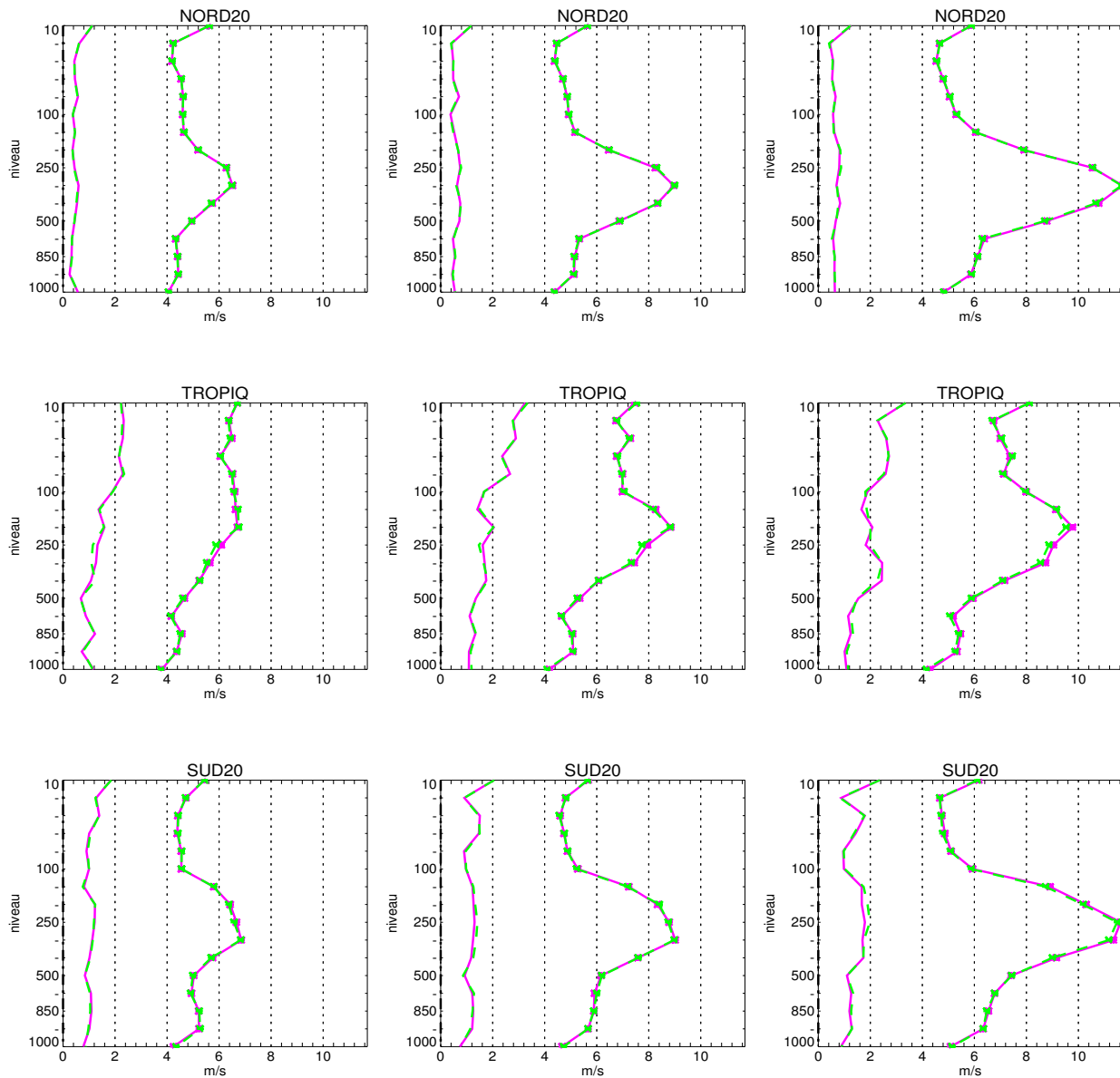


Figure 19: RMS and bias of wind errors from CLOUDDIAG (green) and CONTROL (magenta) experiments. Forecasts are compared to TEMP data. Results are averaged over 10 forecasts (01 to 10 March 2004).

GEOPOTENTIEL

ECH. : / 24 / 48 / 72 /

8 cas, 01/03/2004_00UTC -> 12/03/2004_00UTC

— Biais P701I.r 0/TP

— Eqm P701I.r 0/TP

- - - Biais P703B.r 0/TP

* - - * Eqm P703B.r 0/TP

ECH.24

ECH.48

ECH.72

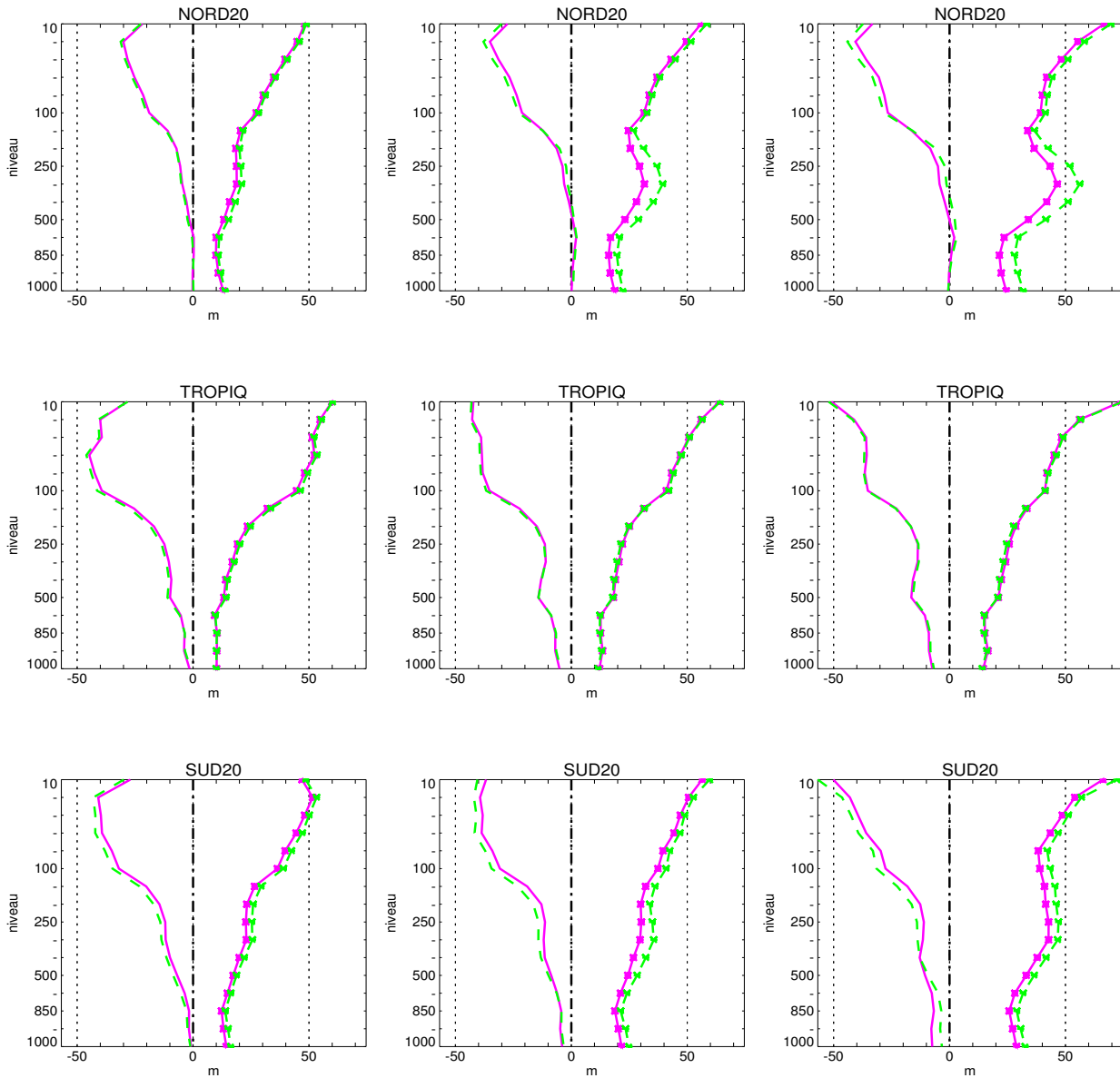


Figure 20: RMS and bias of geopotential errors from CLOUDCO2 (green) and CONTROL (magenta) experiments. Forecasts are compared to TEMP data. Results are averaged over 10 forecasts (01 to 10 March 2004).

TEMPERATURE

ECH. : / 24 / 48 / 72 /

8 cas, 01/03/2004_00UTC -> 12/03/2004_00UTC

— Biais P701I.r 0/TP

— Eqm P701I.r 0/TP

- - - Biais P703B.r 0/TP

* - - * Eqm P703B.r 0/TP

ECH.24

ECH.48

ECH.72

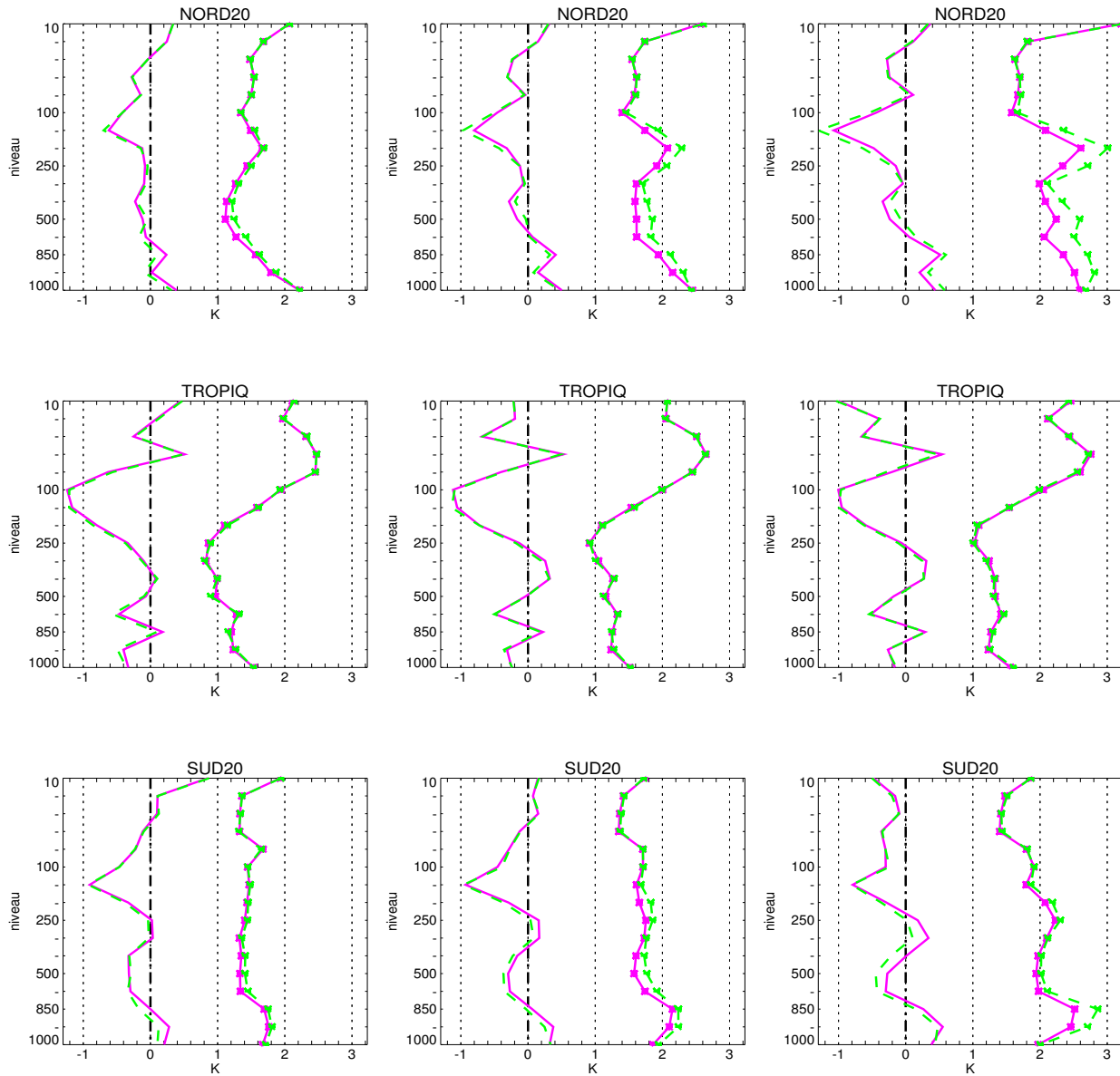


Figure 21: RMS and bias of temperature errors from CLOUDCO2 (green) and CONTROL (magenta) experiments. Forecasts are compared to TEMP data. Results are averaged over 10 forecasts (01 to 10 March 2004).

HUMIDITE

ECH. : / 24 / 48 / 72 /

8 cas, 01/03/2004_00UTC -> 12/03/2004_00UTC

— Biais P701I.r 0/TP

— Eqm P701I.r 0/TP

- - - Biais P703B.r 0/TP

* - - * Eqm P703B.r 0/TP

ECH.24

ECH.48

ECH.72

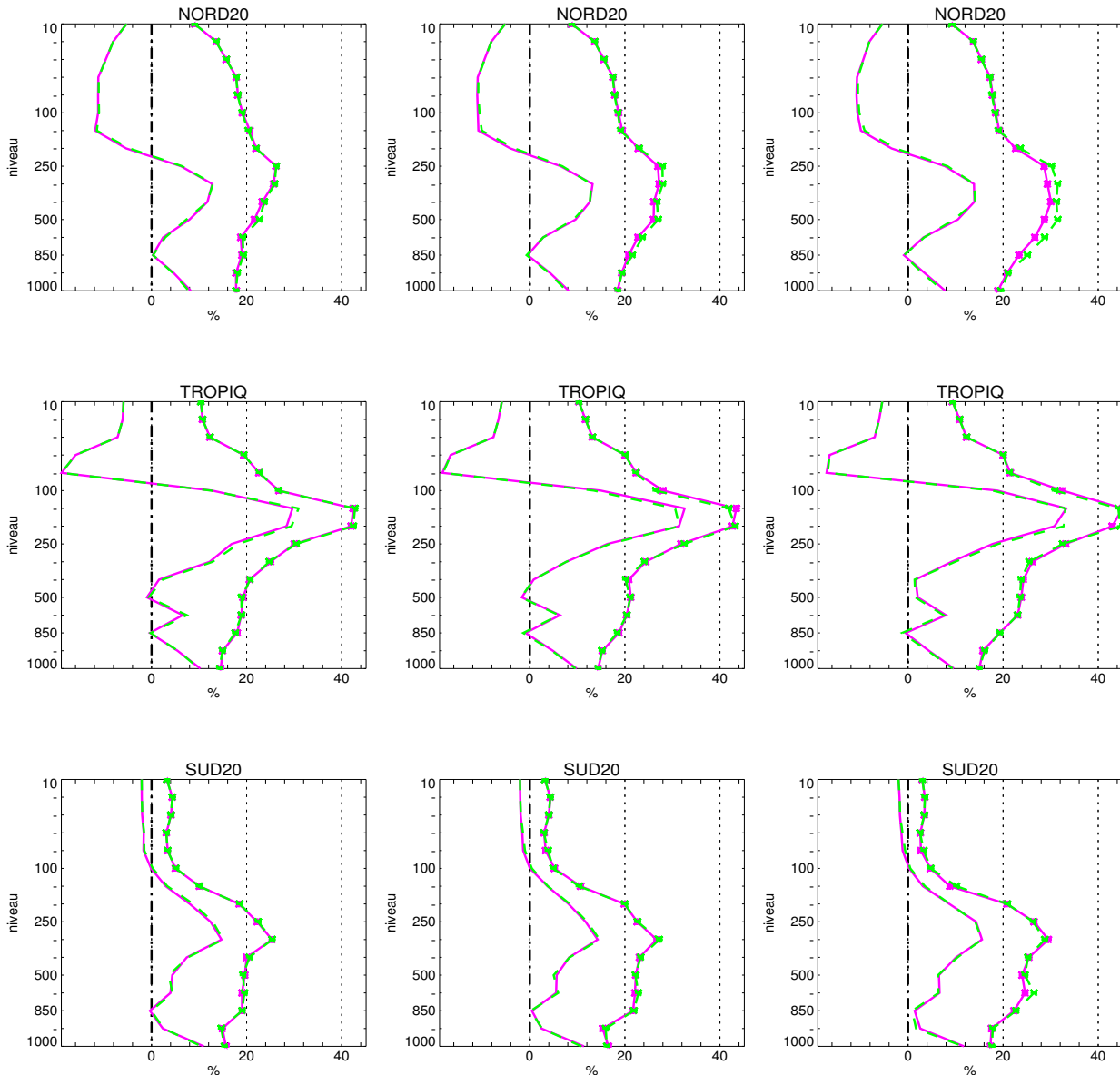


Figure 22: RMS and bias of humidity errors from CLOUDCO2 (green) and CONTROL (magenta) experiments. Forecasts are compared to TEMP data. Results are averaged over 10 forecasts (01 to 10 March 2004).

VENT

ECH. : / 24 / 48 / 72 /

8 cas, 01/03/2004_00UTC -> 12/03/2004_00UTC

— Biais P701I.r 0/TP

— Eqm P701I.r 0/TP

- - - Biais P703B.r 0/TP

* - - * Eqm P703B.r 0/TP

ECH.24

ECH.48

ECH.72

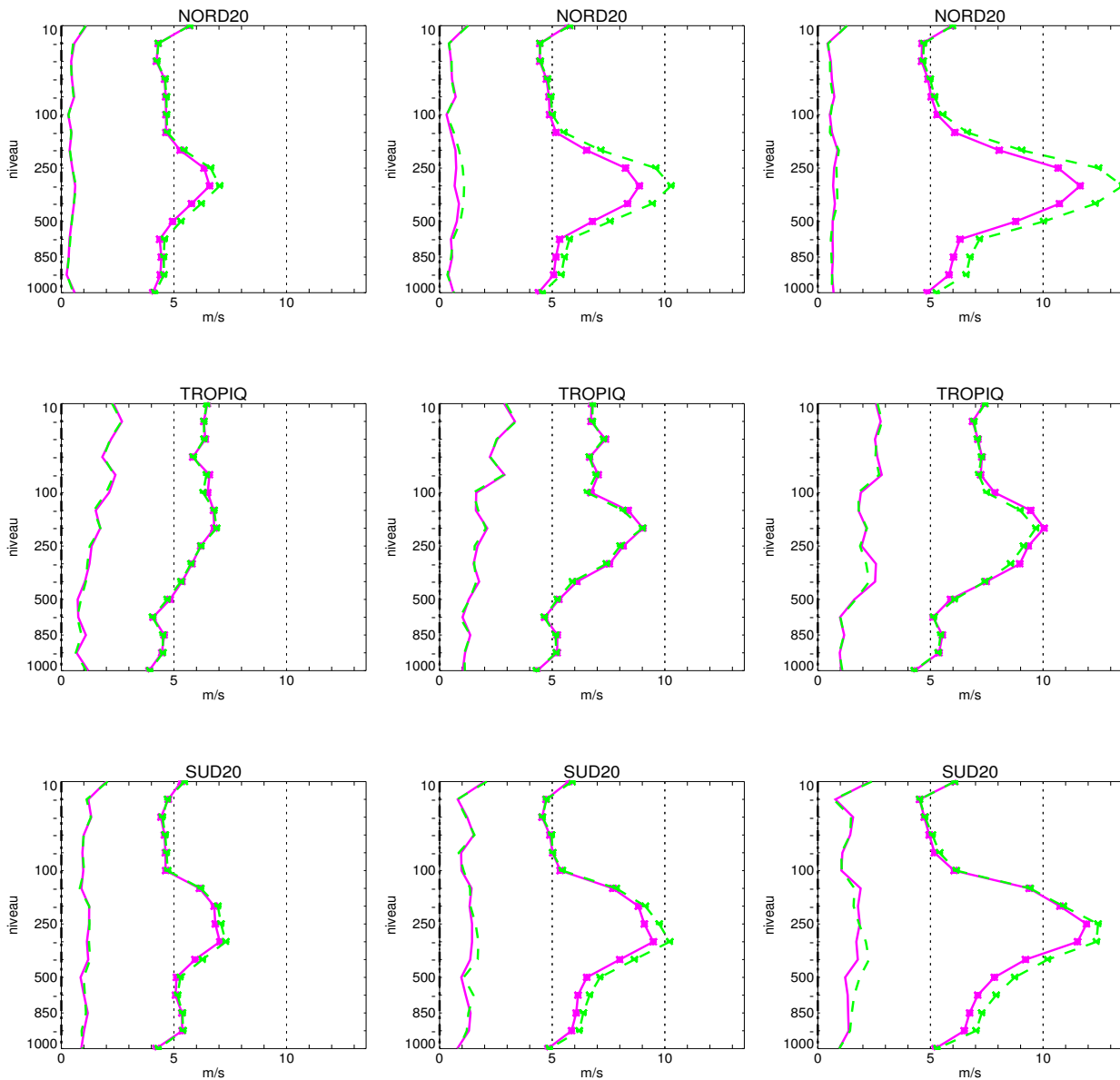


Figure 23: RMS and bias of wind errors from CLOUDCO2 (green) and CONTROL (magenta) experiments. Forecasts are compared to TEMP data. Results are averaged over 10 forecasts (01 to 10 March 2004).

GEOPOTENTIEL

ECH. : / 24 / 48 / 72 /

9 cas, 01/03/2004_00UTC -> 13/03/2004_00UTC

— Biais P701I.r 0/TP

— Eqm P701I.r 0/TP

- - - Biais P702Y.r 0/TP

* - - * Eqm P702Y.r 0/TP

ECH.24

ECH.48

ECH.72

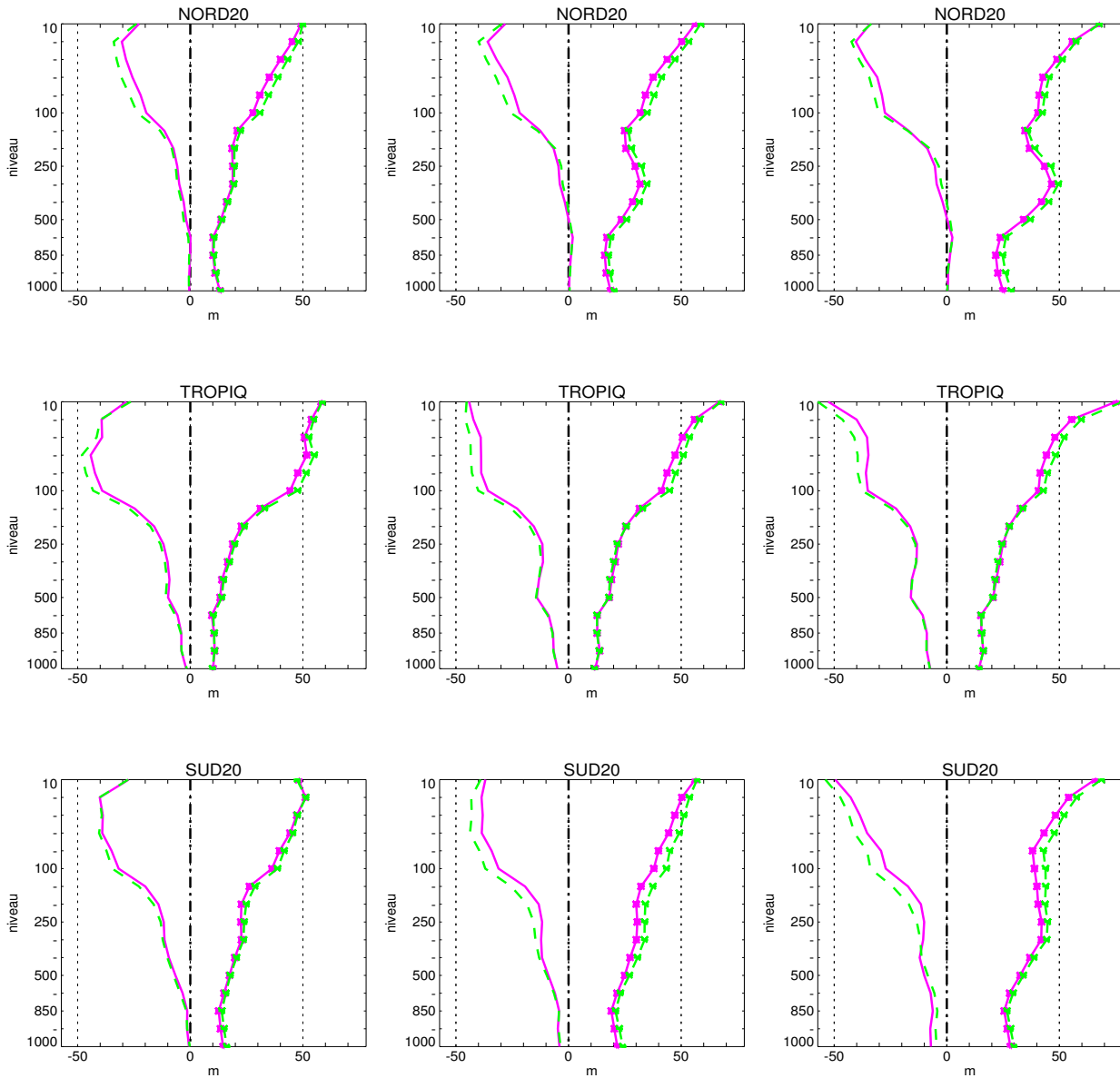


Figure 24: RMS and bias of geopotential errors from CLOUDCO21D (green) and CONTROL (magenta) experiments. Forecasts are compared to TEMP data. Results are averaged over 10 forecasts (01 to 10 March 2004).

TEMPERATURE

ECH. : / 24 / 48 / 72 /

9 cas, 01/03/2004_00UTC -> 13/03/2004_00UTC

— Biais P701I.r 0/TP

— Eqm P701I.r 0/TP

- - - Biais P702Y.r 0/TP

* - - * Eqm P702Y.r 0/TP

ECH.24

ECH.48

ECH.72

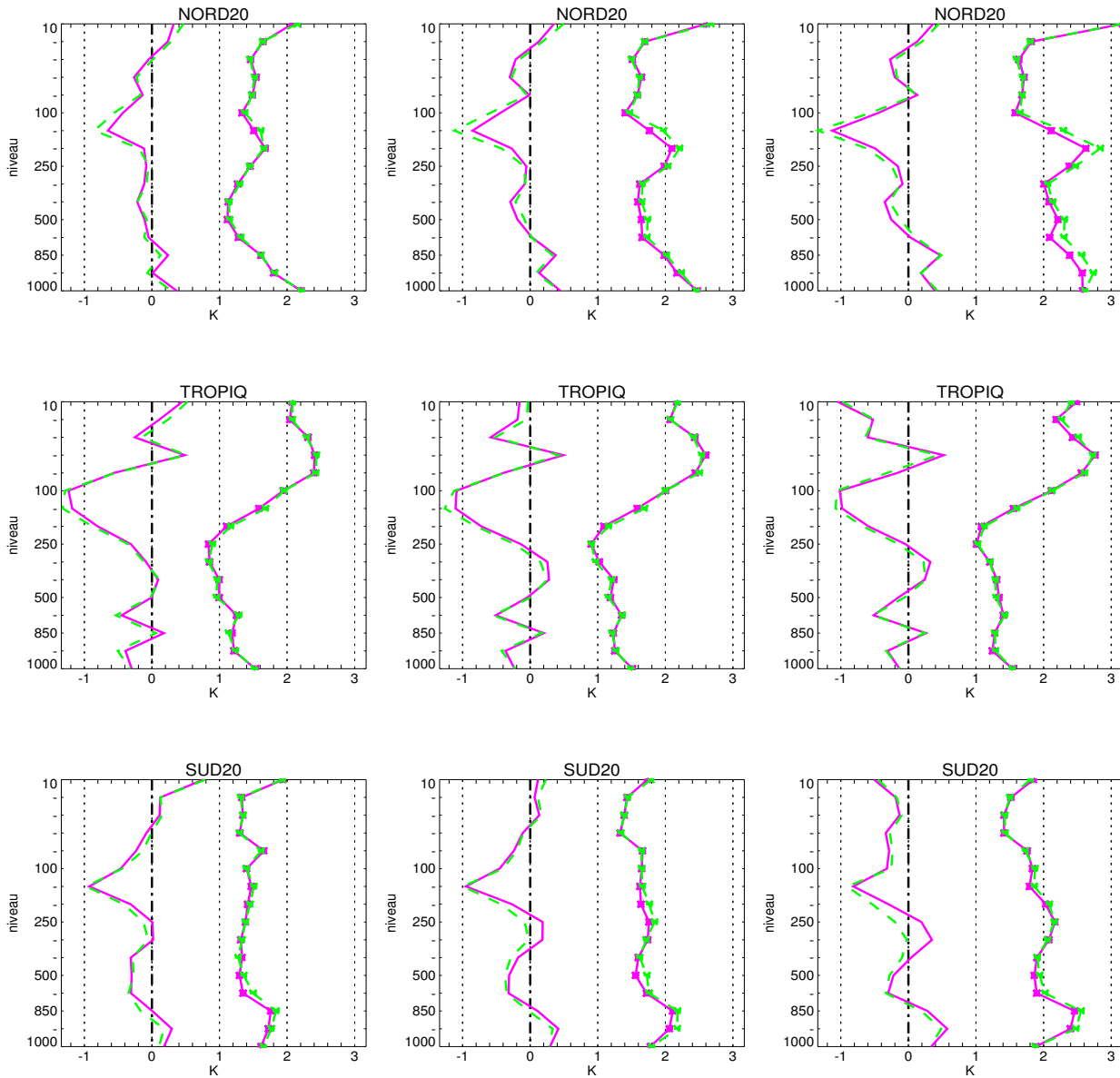


Figure 25: RMS and bias of temperature errors from CLOUDCO21D (green) and CONTROL (magenta) experiments. Forecasts are compared to TEMP data. Results are averaged over 10 forecasts (01 to 10 March 2004).

HUMIDITE

ECH. : / 24 / 48 / 72 /

9 cas, 01/03/2004_00UTC -> 13/03/2004_00UTC

— Biais P701I.r 0/TP

— Eqm P701I.r 0/TP

- - - Biais P702Y.r 0/TP

* - - * Eqm P702Y.r 0/TP

ECH.24

ECH.48

ECH.72

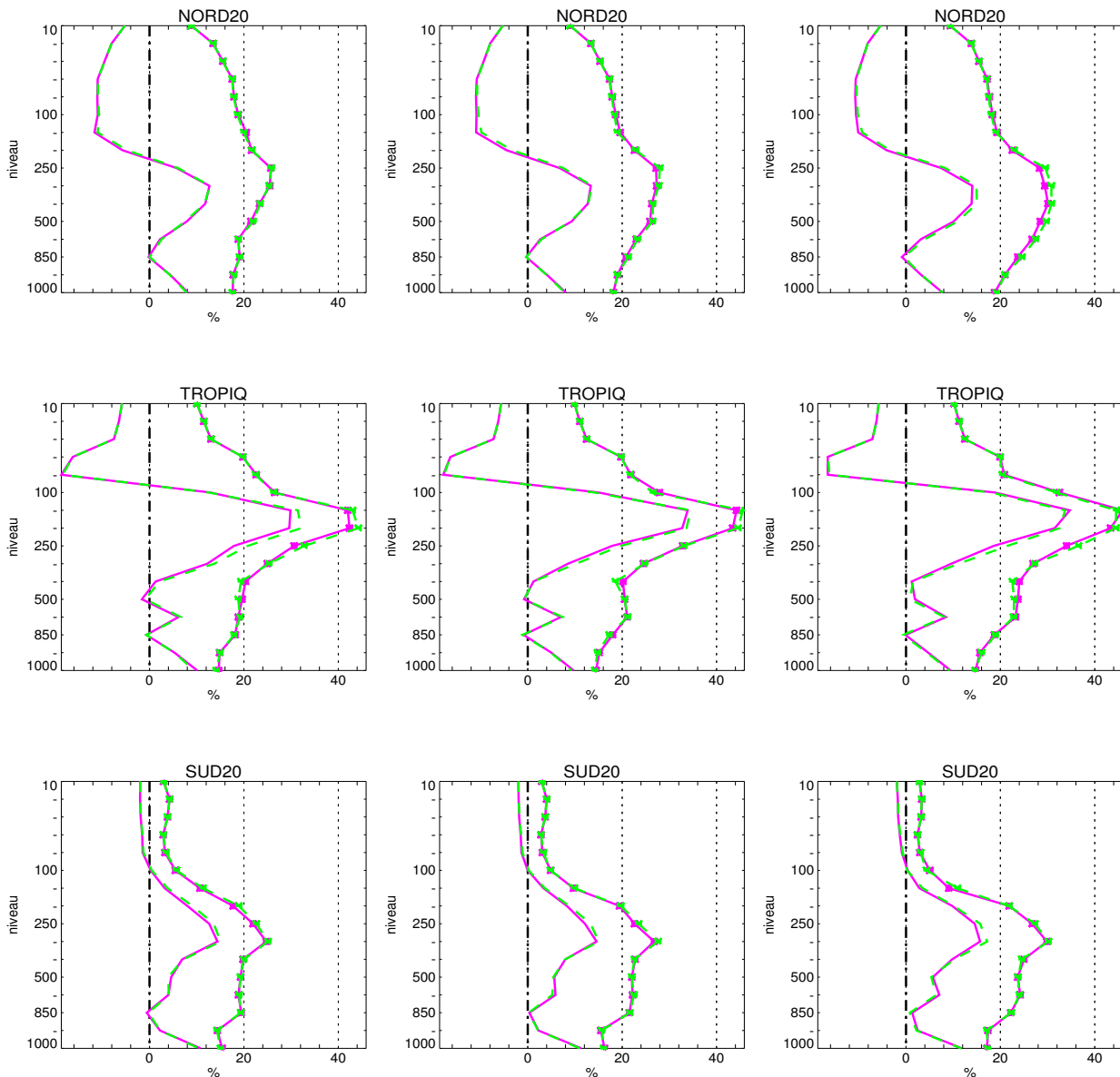


Figure 26: RMS and bias of humidity errors from CLOUDCO21D (green) and CONTROL (magenta) experiments. Forecasts are compared to TEMP data. Results are averaged over 10 forecasts (01 to 10 March 2004).

VENT

ECH. : / 24 / 48 / 72 /

9 cas, 01/03/2004_00UTC -> 13/03/2004_00UTC

— Biais P701I.r 0/TP

— Eqm P701I.r 0/TP

- - - Biais P702Y.r 0/TP

* - - * Eqm P702Y.r 0/TP

ECH.24

ECH.48

ECH.72

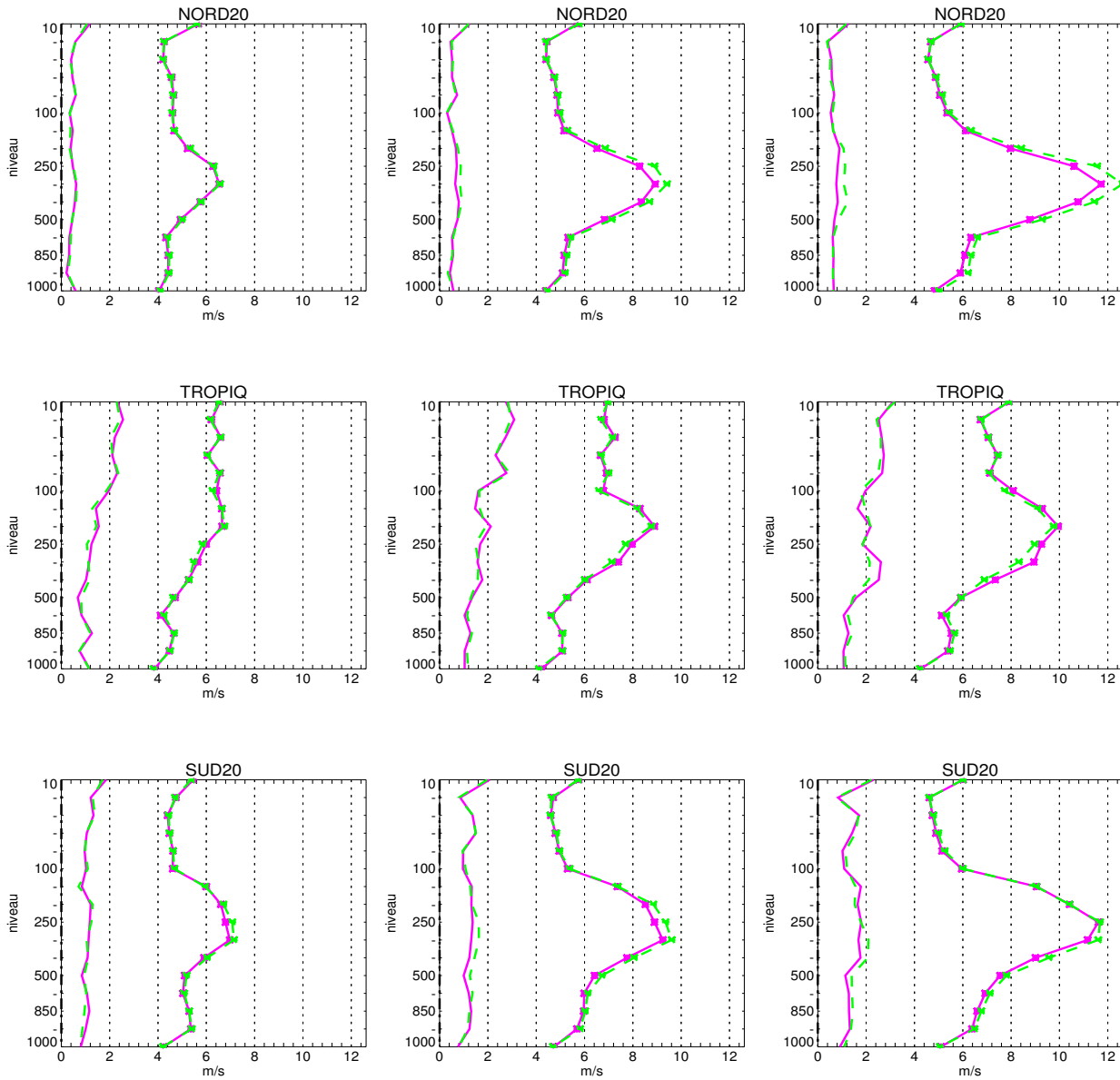


Figure 27: RMS and bias of wind errors from CLOUDCO21D (green) and CONTROL (magenta) experiments. Forecasts are compared to TEMP data. Results are averaged over 10 forecasts (01 to 10 March 2004).